REPORT DOCUMENTATION PAGE

OMB No. 0704-0188

1. AGENCY USE ONLY (Leave blank)	2. REPORT DATE	3. REPORT TYPE AND DATES COVERED
	21 July 1995	Final 10/1/93 - 9/30/95

4. TITLE AND SUBTITLE

The Effects of Suspension of Cohesive Sediments on Shear Stress and Transport

5. FUNDING NUMBERS

N00014-94-1-0012

6. AUTHOR(S)

SCOTT JENKINS, SAIMA AIJAZ, DOUGLAS INMAN

7. PERFORMING ORGANIZATION NAME(S) AND ADDRESS(ES)

Scripps Institution of Oceanography
University of California, San Diego
La Jolla, CA 92093-0209

8. PERFORMING ORGANIZATION REPORT NUMBER

9. SPONSORING/MONITORING AGENCY NAME(S) AND ADDRESS(ES)

Office of Naval Research, Code 1121 OT
Department of the Navy
800 North Quincy
Arlington, VA 22217-5500

10. SPONSORING/MONITORING AGENCY REPORT NUMBER

11. SUPPLEMENTARY NOTES

12a. DISTRIBUTION/AVAILABILITY STATEMENT

No Limitation

13. ABSTRACT (Maximum 200 words)

The variability of rheological properties in fluid-mud suspensions is studied as a function of salinity and sediment concentration. It was found that the steady state shear stress increases exponentially with increasing sediment concentration and increases logarithmically with increasing salinity of the suspension. An analytic model predicting shear stress as a function of electroviscous properties is developed. The model shows that the effect of salts in the suspension is to decrease the zeta potential by compressing the electric double layer, and thereby, elevating the shear stresses acting on the shearing planes at each particle-fluid interface in the suspension. These stresses increase with increasing salt content. The model incorporates the classical double-layer theories of Gouy-Chapman and the Helmholtz-Smoluchowski theory for electrokinetics of charged particles. The model shows good correlation with experimental data at low sediment concentrations where the basic assumptions of the Gouy-Chapman formulation are satisfied. Mixing length arguments show that the elevated shear stresses transport suspended sediment vertically upward across the lutocline, thereby reducing the abundance of suspended sediment directly adjacent to the consolidated bed. This action reduces the deposition rates that were found to obey a power law over several orders of magnitude. This power law was invoked in a vertical advection-diffusion model to calculate the variation in deposition flux with increasing distance along a channel. These calculations were compared with field measurements conducted at two different sites. The calculations based on the power law were found to correctly predict deposition flux behavior in the far field.

14. SUBJECT TERMS	15. NUMBER OF PAGES	16. PRICE CODE
	3 + Appen.	

17. SECURITY CLASSIFICATION OF REPORT	18. SECURITY CLASSIFICATION OF THIS PAGE	19. SECURITY CLASSIFICATION OF ABSTRACT	20. LIMITATION OF ABSTRACT
Unclassified	Unclassified	Unclassified	SAR

FINAL REPORT: THE EFFECTS OF SUSPENSION OF COHESIVE SEDIMENTS ON SHEAR STRESS AND TRANSPORT

Contract No. N00014-94-1-0012

by

Scott Jenkins, Saima Aijaz and Douglas Inman

I) PROJECT SUMMARY

A new and fundamentally different concept for the mechanics of fine-grained cohesive sediment transport is developed here. Suspensions of fine-grained sediments are treated as a magnetio-fluid based upon the presence of weak electric charges on the surface of each sediment particle. These surface charges give rise to Lorentz forces once those particles are set in motion by the fluid flow. These Lorentz forces, termed electroviscous forces, were found to increase the viscosity of the suspension relative to clear water by factors ranging from 3 to 10 at sediment concentrations ranging from 10 to 80 g/l typical of prototype estuaries, harbors, channels and inner shelf coastal waters. These findings were verified in both laboratory and field measurements outlined in the following sections. The strength of the electroviscous effects were found to also be dependent upon salinity and sediment mineralogy vis-à-vis the electrophoretic mobility. These effects were shown to exert a leading order control on scour and erosion of the bottom, with potential applications to dredging, sediment management, and ship wake dynamics in shallow water.

II) RESEARCH GOALS

The research goal of this project was to investigate the dynamic behavior of dense suspensions of fine-grained cohesive sediments to determine where and under what conditions dispersed cohesive sediments can be treated as a magneto-fluid. This hypothesis was proposed because fine-grained sediments (smaller than 40 μm) possess weak surface charges which induce electric and magnetic fields in the fluid suspension when these sediments are set in motion by the fluid. This was an important aspect of the long-term goal of investigating the mechanics of dispersion of fine-grained sediments in the coastal ocean using this magneto-hydrodynamic representations of suspended load.

III) APPROACH AND OBJECTIVES

Our objectives were to formulate the electro-viscous terms of the magneto-hydrodynamic equations of motion so that they can be expressed in terms of measurable sediment and ocean water properties. Laboratory experiments were conducted to validate these formulations and to determine their dynamic shear stress dependence on sediment concentration and salinity. These experiments were also designed to determine the electrokinetic influences on the flocculation process and how these influences effect the particle size distribution. We evaluated the sensitivity of electrokinetic effects in fine-grained suspensions over the range of variability of

sediment and water properties found in the coastal ocean. Finally we incorporated the electrokinetic theory into the advection-diffusion equations and found validation examples for the resulting solutions.

IV) RESULTS

The theory is based on the hypothesis that the first order increase in shear stress is due to the electroviscous properties of small charged sediment particles and not their mechanical interactions vis-à-vis collisions or rubbing together. This theory is detailed in Appendix A and incorporates the classical double-layer Gouy-Chapman approximation and the Helmholtz-Smoluchowski approximation for quantifying the electrokinetics of the charged sediments. Using these approximations, the magneto-hydrodynamic equations of motion are solved analytically for several simple flow geometries. One of these geometries is the co-axial Couette flow typical of many laboratory viscometers. Detailed comparisons are made between these analytic results and experiments conducted in a Brookfield viscometer with UL adapter. These results are contained in Appendices A, B & C. The close agreement of these experiments permitted extension of the electrokinetic theory to the aggregation rate equation (mass continuity) for the flocculation process. Laboratory measurements of floc size as a function of time and salinity for constant shear rates were performed with the aid of a laser particle sizer. The sensitivity of the electrokinetics to sediment properties is parameterized to the lowest order by the electrophoretic mobility; and the electrokinetic dependence on both mineralogy and salinity is also studied by laboratory experiments, as described in Appendices A & C. These results were used to redefine the mixing and vertical advection terms in a river plume and thrust wake dispersion model, described in Appendix D.

The electrokinetic theory has shown a link between the mechanical stress properties of a suspension of mud, silt and clay and the mineralogy, and physical chemistry of those suspensions at fresh, brackish and seawater salinities. At lowest order the theory predicts increases in shear stress with increasing sediment concentration due to the greater abundance of charged particles in relative motion, see Appendix A. Increased sediment concentration increases the density of charged particles in motion, which in turn produces stronger electrostatic and magnetic fields. These stronger fields increase the shear stress required to strain the suspension. The theory shows that mineralogy effects the problem by determining zeta potentials of the charged sediment and that the effect of salts on these suspensions is due to the decrease in zeta potential as elevated salts compress the electric double layer which envelopes the charged silts and clays. Compression of the double layer elevates the shear stresses acting on the shearing planes over each particle-fluid interface in the suspension. These stresses increase with increasing salt content. These processes were found to be relatively independent of pH effects in seawater. The increased floc-to-floc stress transfer induced by the electrokinetics was found to limit both the largest medium floc size and the rate at which that size is achieved, as found in detail in Appendices A & C. These flocs are rather fragile, and the electrokinetic effects are found to regulate the floc breaking processes. Both the enhancement of shear stress and the regulation of floc size are found to be most sensitive to the electrophoretic mobility of the sediment mineral types, see Appendix A. For a given mineral type, we are able to model the dependence of the electrophoretic mobility on salinity. The data scatter is due to mineral variations in the sediments of the different coastal areas. When the shear stress enhancements

are accounted for in the diffusion terms, and the flocculation sizes are used to prescribe settling velocities for vertical advections terms, a realistic scour is calculated as found in Appendix D.

V) PUBLICATIONS

The following is a list of the publications that were produced under this contract (N00014-89J-117):

Aijaz, S., & S.A. Jenkins, 1994, "On the electrokinetics of shear stress behavior in fluid-mud suspension", *Jour. Geophys. Res.*, v.99, n. C6, pp. 12,697-12,706.

Jenkins, S.A., S. Aijaz, and J. Wasyl, 1993, "Transport of fine sediments by hydrostatic jets," in A.J. Mehta (ed.), *Nearshore and Estuarine Cohesive Sediment Transport*, Amer. Geophysical Union, v.2, pp. 331-347.

Aijaz, S., & S.A. Jenkins, 1993, "Dynamics of shearing in flocculating fine sediment suspensions", *Die Makromolekulare Chemie, Proceedings of the 11th Polymer Networks Group Meeting*, September 1992, San Diego, Huthig and Wepf Verlag, German, in press.

Aijaz, S., & S.A. Jenkins, 1993, "Fluid-sediment interactions and dynamic shear stress in fine sediment suspensions", *Proceedings of the Second International Conference on Micromechanics of Granular Media*, July, 1993, Birmingham, UK, Balkema, Rotterdam, in press.

Aijaz, S., S.A. Jenkins, & D.L. Inman, 1993, "Dynamic shear stress in fluid-mud suspensions", *University of California, San Diego*, Scripps Institution of Oceanography, SIO Reference Series, n. 93-23, 106 pp.

Aijaz, S., "Dynamic shear stress in fluid-mud suspensions", 1993, Ph.D. dissertation, S.A. Jenkins & D.L. Inman, Chairmen, *University of California, San Diego*, 147 pp.

APPENDIX A

ON THE ELECTROKINETICS OF SHEAR STRESS BEHAVIOR IN FLUID-MUD SUSPENSIONS

Saima Aijaz and Scott A. Jenkins

JOURNAL OF GEOPHYSICAL RESEARCH, VOL. 99, NO. C6, PAGES 12,697–12,706, JUNE 15, 1994

On the electrokinetics of shear stress behavior in fluid-mud suspensions

Saima Aijaz and Scott A. Jenkins

Scripps Institution of Oceanography, University of California, San Diego

Abstract. The variability of rheological properties in fluid-mud suspensions is studied as a function of salinity and sediment concentration. It was found that the steady state shear stress increases exponentially with increasing sediment concentration and increases logarithmically by increasing the salinity of the suspension. An analytic model predicting shear stress as a function of electroviscous properties is developed. The model shows that the effect of salts in the suspension is to decrease the zeta potential by compressing the electric double layer and, thereby, elevating the shear stresses acting on the shearing planes at each particle-fluid interface in the suspension. These stresses increase with the increase in salt content. The model incorporates the classical double-layer theories of Gouy-Chapman and the Helmholtz-Smoluchowski theory for electrokinetics of charged particles. The model shows good correlation with experimental data at low sediment concentrations where the basic assumptions of the Gouy-Chapman formulation are satisfied. At progressively higher sediment concentrations, there are increasingly larger departures between the model predictions and the experimental data due to violations of these basic assumptions. The advantages and limitations of the model are discussed.

Introduction

Most of the dredging performed worldwide to maintain deep draft harbors and waterways involves removing muds comprised of cohesive sediments. Without the annual $2 billion expenditure for maintenance dredging, these harbors and waterways would become useless. Recent sedimentation control experiments in deep-draft shipping berths have succeeded in retarding or preventing fine sediment deposition by employing jets and wings to resuspend the layer of fluid-mud formed adjacent to the immobile consolidated bottom [*Jenkins and Bailard,* 1989; *Jenkins and Wasyl,* 1990]. In these experiments, the shear stress of the fluid-mud suspension was found to be the leading order parameter which determines the size and power requirements of the various systems tested [*Jenkins et al.*, 1993]. The shear stress also plays a controlling role in limiting the amount of resuspension of fluid-mud because of the vertical eddy diffusion in natural estuarine circulation [*Mehta*, 1989]. Shear stresses acting on the sediment layers may also be related to their erosion rates [*Partheniades*, 1965].

The shear stress, together with the grain- size distribution and sediment concentration are among the most important properties in characterizing the shoaling conditions in estuaries and shallow seas. From an engineering and hydraulic standpoint, the determination of these properties would aid in planning and interpretation of field measurements of fine sediment transport. These in turn would help in establishing design criteria for the control of shoaling in navigation channels, harbors, and wetland restoration projects.

Paper number 94JC00285.
0148-0227/94/94JC-00285$05.00

The steady state shear stress induced in a fine cohesive sediment suspension is commonly believed to result from friction due to the relative motion and interaction of the fluid and the sediment particles in a time invariant flow [*Dyer*, 986; *Lambermont and Lebon,* 1978]. It has also been attributed to the stress required to break the bonds within aggregates of sediment particles during shearing [*Krone*, 1962]. Unlike coarse sediments, the fine sediments do not behave as individual units but are bound together as flocs. Flocculation takes place when sediment-laden freshwater mixes with seawater containing salts. In freshwater where there are no ionic solutions, the fine silt and clay particles carry a large electric double layer compared to their radii. The electric double layer constitutes the charge of the particles and an equivalent amount of counterions. As the freshwater mixes with seawater, the cations in the salts are attracted toward the surface of the particle. Some of these neutralize the charge on the particle, resulting in compression of the double layer. The compaction of the double layer causes the electric potential at the shearing plane between the solid-liquid interface (known as the zeta potential) to drop rapidly. The repulsive forces become small and the particles can approach each other to form flocs. *Gripenberg* [1934] and *Whitehouse et al.* [1960] have shown that for sediment concentrations less than 10 g/L, flocculation occurs very rapidly when salinity is increased to 1 and 3 parts per thousand (ppt) and ocurrs gradually thereafter. The forces responsible for the chemical bonding that holds the particles together are believed to be the electrochemical forces arising because of the electrically charged particles. Chemical bonding results from isomorphic substitutions in the clay crystal lattice or from adsorption of ions from a salt solution onto a sediment particle [*van Olphen,* 1977].

If floc-breaking processes are important in determining the shear stress, then another set of mechanisms, "biophysical mechanisms" [*Bennett et al.*, 1991] must also be considered. *Pierce and Siegel* [1979] have observed that the major portion of suspended solids in estuarine waters is composed of

aggregates of mineral grains, soft organic matter, biogenic debris, and phytoplankton. Biogenic influences such as the pelletization through filter-feeding organisms or secretions of organisms bind the sediment together [*Zabawa,* 1978]. *Rashid et al.* [1972] emphasize the role of saline waters in promoting flocculation. Their experiments show that the presence of dissolved salts in the water column enhances the adsorption of organic matter on fine sediments, leading to flocculation.

A large number of investigators [*Williams and Williams,* 1989; *Hunter,* 1982; *Rand and Melton,* 1977] have studied the flow behavior of flocculated suspensions and have proposed models by computing interaction energies between two particles of specified geometries. All such previous work has been done either on pure clay minerals or on colloidal suspensions. The present work seeks to determine the behavior of the shear stress of naturally occuring sediment suspensions as found in bays and estuaries. These suspensions are studied, both with and without the presence of organic matter. We proceed from experimental findings of *Aijaz* [1989], which have shown that the shear stress increases with increasing salinity (NaCl content). Regardless of the presence or absence of organic matter, one possible interpretation of these results is based on the aforementioned studies on interparticle friction and floc- breaking. However, this paper will explore a new hypothesis that these variations in shear stress are related to electrokinetic properties associated with the charged particles that make up the flocs. The net charge on a sediment particle is salinity dependent owing to the electric double layer around its surface. These charged particles are set into motion by the moving suspension. This motion generates large numbers of electric and magnetic fields. Relative motion between the charged particles gives rise to electromagnetically induced traction forces. This electromagnetic traction might therefore enhance the shear stresses, especially at high salinities.

The following sections will describe the methods and procedures adopted to measure the steady state shear stress, the zeta potential, and the floc sizes in suspensions of naturally occuring fine-grained sediments. These are studied at varying salinities and sediment concentrations. Finally, a model is proposed which describes how the shear stress is controlled by site specific sediment and water column properties. The importance of zeta potential on sediment rheology and dynamics is emphasized.

Experiment Setup

Sediment Characteristics

The sediment samples were collected from Mission Bay in San Diego, California. The samples were obtained near the mouth of Rose Canyon at a location approximately 30 m into the bay. The divers took the samples by diving at a depth of 3 m into the water and scooping up the sediment in plastic containers. The samples were stored at 4°C in a dark room. All experiments were conducted within 4 or 5 days of sample collection to minimize the effects of diagenesis during storage. The sediments were composed of 13% clay, 77% silt, and 10% sand, with an organic content of 3%. The predominant minerals present in the sediment were montmorillonite (44%), illite (48%) and kaolinite (8%).

The mineralogical composition was determined by X -ray diffraction analysis. The sample was filtered through 0.45 μm filter; the filter was subsequently mounted on a glass slide and analyzed on the X -ray diffractometer using Cu K-α radiation at 40 kV and 20 mA. The types of minerals were identified by comparison with the patterns of standard minerals.

The organic content was determined by means of a carbon-hydrogen-nitrogen (CHN) analyzer. The CHN analyzer measures the carbon content, which may be taken as a measure of the organic content [*Meade,* 1972].

Sediment Rheology

A Brookfield Synchro-Lectric viscometer, equipped with a special UL adapter was used to measure the shear stresses produced in the sediment suspension. The usefulness of this instrument in evaluating the dynamic behavior of cohesive sediments both in field and laboratory has been described in detail by *Faas* [1990].

The Brookfield viscometer measured the shear stress by sensing the torque required to rotate a spindle at a constant shearing rate while immersed in a fluid-sediment suspension. The coaxial cylinder geometry of the UL adapter provided greater sensitivity for low-viscosity fluids than an ordinary viscometer with a large gap between spindle and container. The instrument was accurate to within 1% of the full-scale reading. It was chosen because of its precision and its ability to evaluate the rheological behavior of the cohesive sediment suspensions as they respond to the stresses within the environment. *Rosen* [1972] and *Heugen and Tung* [1976] have described techniques to characterize the rheological properties of emulsions and polymer solutions using Brookfield viscometers with coaxial geometries. With these techniques, we established well-defined shear rates for the corresponding rpm settings of a Brookfield Synchro-Lectric viscometer.

The shear stress is calculated using the basic principles of rotational viscometry [*Eirich,* 1960]. In a rotating coaxial viscometer (with the UL adapter), there is an inner rotating cylinder, the spindle (measuring 25.15 mm in diameter), and an outer stationary cylinder (measuring 27.62 mm in diameter). The annular space (2.4 mm in width) between the two coaxial cylinders is filled with the fluid-sediment suspension. The actual length of the inner cylinder is 90.74 mm and the effective length is calculated as 92.39 mm. The effective length includes corrections for end effects. The correction for end effects is very small because the surface area of the annulus gap is small compared to the vertical surfaces. If the applied torque to the spindle is M, and the tangential shear stress on the cylindrical surface is τ, then a torque, M, results from the tangential traction on the spindle. The torque, M is shown as a dial reading on the viscometer, and may be written as:

$$M = 2\pi r_b^2 L \tau \tag{1}$$

Therefore shear stress is given from (1) as

$$\tau = \frac{M}{2\pi r_b^2 L} \tag{2}$$

The shearing rate is calculated as

$$s = \frac{2\,\omega\, r_c^2}{r_c^2 - r_b^2} \tag{3}$$

where r_c^2 is the radius of the outer cylinder, r_b^2 is the radius of the inner cylinder, ω is the rotation speed in rad/s, and L is the

effective length of the inner cylinder. Equation (3) is derived specifically for coaxial cylinder geometry [*Van Wazer et al.*, 1963]. When using the Brookfield viscometer with a spindle immersed in a beaker (having a relatively larger gap), the equation for calculations of shearing rate and shearing stress would asymptotically approach the case of a rotating cylinder in an infinite fluid which has an algebraically different solution. By using the UL adapter with a small gap between the inner and outer cylinder, the gap size did not exceed the critical radius conditions. When the suspension exhibited a yield stress, the critical radius calculated [*Van Wazer et al.*, 1963] was always greater than the actual gap size.

Figure 1 shows the rheology of the sediment suspension. The shear stress was measured at varying shearing rates from 0.732 s^{-1} to 74.42 s^{-1}. The suspension exhibits a pseudoplastic or shear-thinning behavior, which is typical of aqueous suspensions of clays or natural sediments [*Bryant et al.*, 1980; *Williams*, 1986].

Shear Stress Measurement Procedures

The experimental method consisted of washing the sediment sample with deionized water to remove the sea -salts and screening the sample to remove pieces of debris, shells, etc. The sample was then sieved through a 62 μm sieve to separate the fine fraction from the coarse sediment fraction. The suspension was agitated thoroughly, either by vigorous hand- shaking or mixing in an electric blender to break any large clumps or flocs. The suspension was sheared in the Brookfield viscometer, operated at 60 rpm. This speed provided a shearing rate of 74.4 s^{-1} using (3) and was kept constant for all experiments. The initial reading was taken at zero salinity. Subsequent readings were taken at increasing salinities up to 30 ppt. Salinity was represented by NaCl in parts per thousand (ppt). To check the performance of the instrument and the reproducibility of data, three separate runs were made on the same sediment suspension and at least three viscometer readings were taken for each increment of salinity. The shear stress was measured at a fixed sediment concentration, while the salinity was varied in increments of 5 ppt. The experiments were then repeated for varying sediment concentrations.

Two sets of experiments were conducted. One consisted of analyzing the shear stress behavior of a natural sediment sample, and the other measured the shear stress after removing the organic matter from the sediment sample. The organic matter was removed by treating the sediment sample with 30% hydrogen peroxide solution to oxidize the organic matter present in the sediment [*Jackson*, 1969].

Shear Stress Results

The results show a very consistent pattern with the change in sediment concentration. The shear stress rises exponentially with the rise in sediment concentration (Figure 2). The increase in the shear stress is significant, considering that the shear stress for clear water at 20°C is only 0.67 dyn/cm^2 for a shearing rate of 74.4 s^{-1}. Although the exponential rate is intriguing, the general tendency of the shear stress to increase with the sediment concentration is a well-known result [*Einstein and Krone*, 1962; *Krone*, 1984; *Das*, 1970]. Generally, it is believed that as the number of particles in the suspension increases, there is a greater probability of interparticle collisions, resulting in more flocs being formed. With more flocs, more fluid is entrained, thereby promoting shear stress transfer throughout the suspension. Thus there is a growth in shear stress.

The relationship between salinity and shear stress for natural sediments is shown in Figure 3. As the salinity is increased from 0 to 3 ppt, there is a sharp increase in the rise in shear stress, followed by a gradual increase beyond 3 ppt. This behavior is in agreement with the results of previous investigators in the lower-salinity range. [*Whitehouse et al.*, 1960; *Edzwald et al.*, 1974; *Gibbs*, 1983]. However, there are no comparable previous results in the higher-salinity range. Even after 3 ppt, the shear stress does not level off but continues to increase with increasing salinities. Several runs of experiments were conducted in the sediment concentration range of 10 g/L to 75 g/L. The values of shear stress varied from 0.85 dyn/cm^2 at 10 g/L and zero salinity up to 5 dyn/cm^2 at 75 g/L and 30 ppt. The shear stress for the sediment concentration of 75 g/L increases from 1.56 dyn/cm^2 at zero salinity to 4.26 dyn/cm^2 at 3 ppt to 5.06 dyn/cm^2 at 30 ppt. (Figure 3). There is a 19% increase in shear stress from 3 ppt

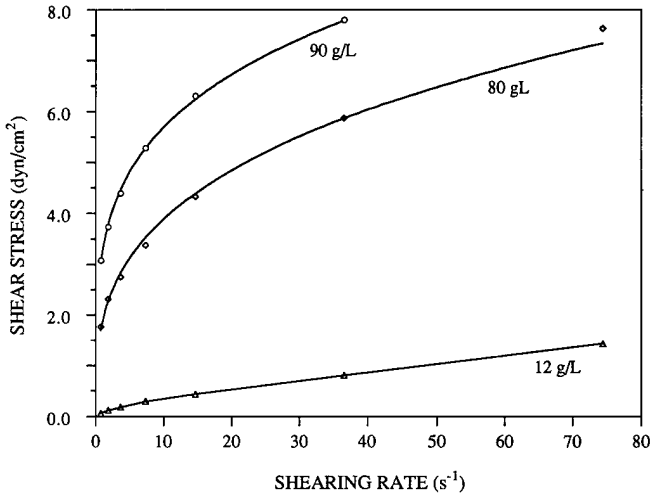

Figure 1. Rheology of fluid-mud suspension.

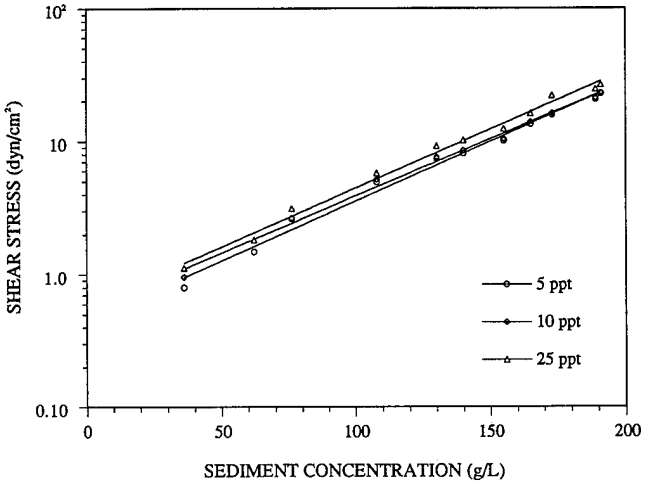

Figure 2. Exponential dependence of shear stress on sediment concentration shown at salinities of 5,10, and 25 ppt.

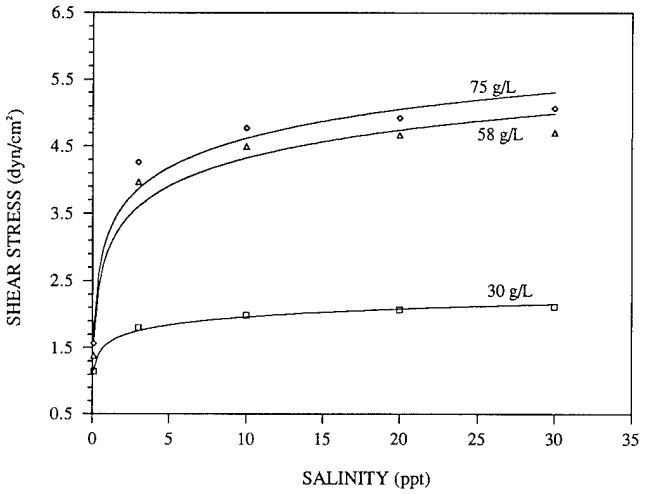

Figure 3. Dependence of shear stress on salinity for natural sediments shown at sediment concentrations of 32, 58, and 75 g/L.

to 30 ppt. Similarly, other runs show a percentage increase of 15 to 20% as the salinity increases from 3 to 30 ppt. The sediment without the organic matter (Figure 4) shows the same trend as the natural sediments. This result suggests that the electrochemical forces play a dominant role in the organic as well as inorganic particle interactions and floc- formation. In the presence of organic matter, the cations in the surrounding water serve as a linkage between humic material and clay minerals [*Rashid,* 1985]. The increased cations in solution resulting from increased salinity reduce the electrostatic repulsion caused by the similarity of charges of clay minerals and organic compounds, thereby allowing closer approach of the reactants. This enhances the physical interaction between clay minerals and humic compounds. With increased physical adsorption, conditions improve for chemical bonding between the functional groups of humic acids and the charge sites of clay minerals. The zeta potential across the double layer is reduced because the adsorption of organic matter causes displacement of adsorbed counterions [*Stumm and Morgan,* 1981]. This leads to increased shear deformations, which in turn increase the shear stress in the suspension. Since both the sediment particles and the organic matter carry a net negative charge in suspension, the effect of salts is similar in both cases. Hence we see similar patterns in the behavior of shear stress due to salinity variations in natural sediments as well as in sediments without the organic matter (see Figures 3 and 4).

Electrophoretic Mobility Measurements

The electrophoretic mobility (rate at which the particles move under an applied electric field) of sediment particles was measured by a Laser Zee model 501 (Pen Kem, New York). This instrument measures the electrophoretic mobility of particles by the technique of microelectrophoresis. The electrophoretic mobilities are converted to zeta potential values by the Helmholtz-Smoluchowski equation. Corrections are applied for the viscosity and dielectric constant of the medium. This instrument has an advantage over conventional instruments in that there is no need to use a stopwatch to time the particles as they move toward the electrode. In conventional instruments, 20 to 40 particles are timed individually and the results averaged to give a single measurement. The Laser Zee utilizes a unique prism technique that makes the moving particles appear stationary and thus only a single measurement is required. This method is much more accurate than the older method. The electrophoretic mobility of particles was measured at varying salinities from 0 to 20 ppt. The instrument did not give stable measurements above 20 ppt. The measured values at these salt concentrations are in close agreement with those of *Hunter and Liss* [1979], who measured the electrophoretic mobilities of suspended particles from estuarine and coastal waters. Their instrument utilizes Ag/AgCl electrodes to allow determination in full strength seawater.

Figure 5 shows the measurements of electrophoretic mobilities (u_e) of sediment particles from different bays and estuaries. The data from Mission Bay is from the present study. The rest of the data has been replotted from *Hunter and Liss* [1979]. A polynomial curve is fitted to the entire data set and linear regression gives the coefficient of correlation to be

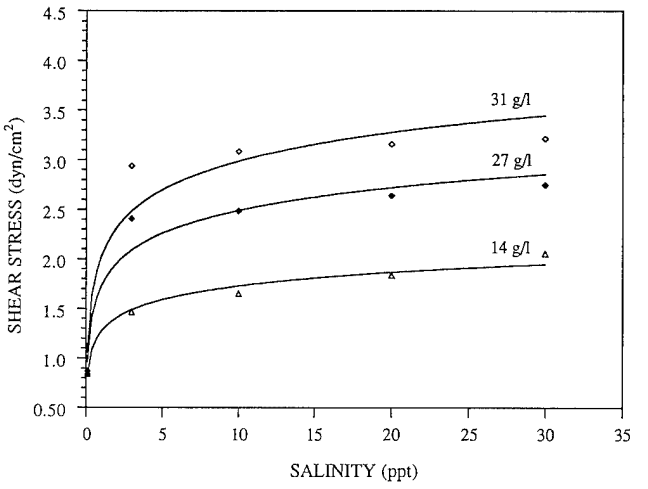

Figure 4. Relationship between shear stress and salinity for sediments without organic matter at varying sediment concentrations.

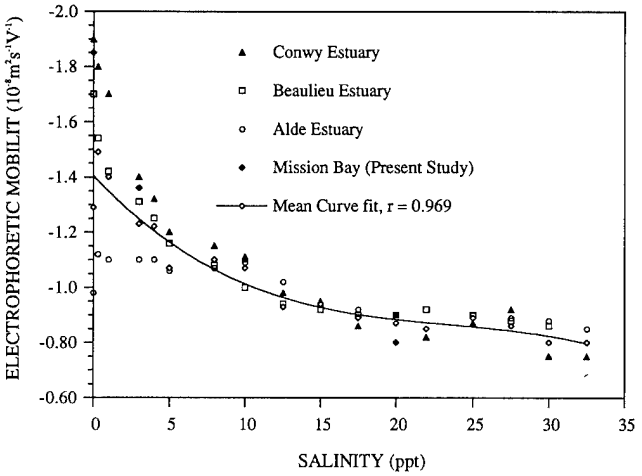

Figure 5. Electrophoretic mobilities of particles at varying salinities. Data for Conwy, Beaulieu and Alde estuaries replotted from *Hunter and Liss* [1979].

0.969. The values of zeta potential were calculated from the electrophoretic mobilities obtained from the polynomial fit. The data show measured mobilities of particles collected from a number of estuaries with varying contents of divalent and polyvalent ions. It is observed that the electrophoretic mobility of sediment particles steadily declines with increasing salinity. *Williams and Williams* [1978] determined the electrophoretic mobilities of kaolinite particles at varying *p*H and found that above *p*H 5 (which is typical of estuarine waters), the electrophoretic mobility decreases with an increase in the molar concentration of NaCl. This decrease in mobility or surface charge of the particles is attributed to the electric double-layer compression. At high salinities, the natural electrokinetic charge of the particles will be neutralized by incorporation of the cations into the fixed part of the double layer. However, at low salinities, the concentration of cations is not high enough to completely compress the double-layer. Hence the electrokinetic charge is much higher at low salinities and steadily decreases as salinity increases. The electrophoretic mobilities from different sites (Figure 5) ranged from -1.9×10^{-8} to -1.2×10^{-8} $m^2V^{-1}s^{-1}$ at near zero salinity and from -8.3×10^{-9} to -8.9×10^{-9} $m^2V^{-1}s^{-1}$ at 30 ppt salinity. The measurements from Conwy and Beaulieu Estuaries show a sharp decrease in electrophoretic mobility as the salinity increases, whereas the measurements from Alde Estuary show a more gradual decrease of electrophoretic mobility over the salinity range from 0 to 35 ppt. The reason is that the Alde Estuary has a much higher content of divalent and polyvalent cations than the other two estuaries. The polyvalent cations are more efficient in compressing the double layer than monovalent ions. Therefore particles from Alde Estuary have a lower charge at all salinities than the other estuaries. Data from the present study (Mission Bay) closely resembles that from Conwy and Beaulieu Estuaries. This close agreement is clearly expected because the only type of cations present in the salt used in the experiments consisting of sediment from Mission Bay were the monovalent Na^+ ions. Hence these show a dramatic decrease in the electrophoretic mobility as the salt content increases.

Floc Size Measurements

These were difficult measurements owing to the fragile nature of the flocs. Special techniques were utilized which minimized the breaking or altering of the floc structure. Previous attempts to measure floc size by using scanning electron microscopy (SEM) and an optical microscope were not successful. SEM requires that the sample be dried prior to installation in the instrument. In previous attempts, the sample was air-dried which caused a collapse in the structure of the flocs. To overcome these difficulties, the laser diffraction particle size analyzer was used for measuring floc sizes. This instrument had an advantage in that the sediment sample was observed in a suspended state. Therefore there was minimum disturbance or destruction of flocs. Numerous investigators [*Butters and Wheatley*, 1982; *Burban et al.*, 1989; *McCave et al.*, 1986; *Singer et al.*, 1988] have used laser sizers to determine particle sizes in suspension.

The laser sizer works on the principle that the particles of a given size diffract light through a given angle, this angle increases with decreasing particle size. The size distribution is obtained by calculating the angular distribution of the light scattering.

The sample was washed with deionized water to remove sea-salts. It was exposed to ultrasound to break up particles which were stuck together. Samples of varying salinities were prepared. Each sample was poured into the sample chamber. From the sample chamber, the sample flowed into a sample cell where the actual measurement took place. The sample chamber contained a stirrer to keep the particles in suspension and a circulating pump to circulate the sample to and from the sample cell. The speed of the stirrer and the circulating pump was adjustable. Great care was taken to choose the optimum stirring speed. If the speed was too high, then the flocs would break apart. If the speed was too low, then the flocs would settle out of suspension. Similarly, the circulating pump speed had to be chosen such that it was not too high to tear the flocs nor too low to allow a buildup of particles in the circulating system. The speeds selected were kept constant throughout all the experiments.

The initial size distribution at zero salinity is shown in Figure 6, where the median particle diameter is 7.3 μm. The subsequent floc size results indicate an increase in the median diameter of the flocs as the salinity increases from zero to 25 ppt (Figure 7). Above 25 ppt, the median floc diameter either levels off or decreases slightly. The apparent decrease in particle size at higher salinities may, however, be an artifact of the experimental method. As the flocs get bigger, the limited clearances between the impeller and the liner of the circulating pump could be causing the flocs to break. Because of this instrument limitation, quantified relationships between floc- size and salinity could not be obtained at high salinities. The actual floc- size distribution at increasing salinities is shown in Figures 8(a) through 8(c).

All the above experiments did not duplicate the specific ionic composition of seawater. Instead, NaCl was used to represent salinity. Any possible *p*H effects arising from not using natural seawater appear to be negligible. As discussed in the following section, the electrokinetics of the shear stress is controlled to the lowest order by the conductance of the particular ionic constituents. Besides Na^+ ions, those ions found in seawater that would have the greatest effect on conductance are the hydrogen and the carbonate and bicarbonate ions. Now, the H^+ ion concentration of an air saturated NaCl solution in deionized water is approximately

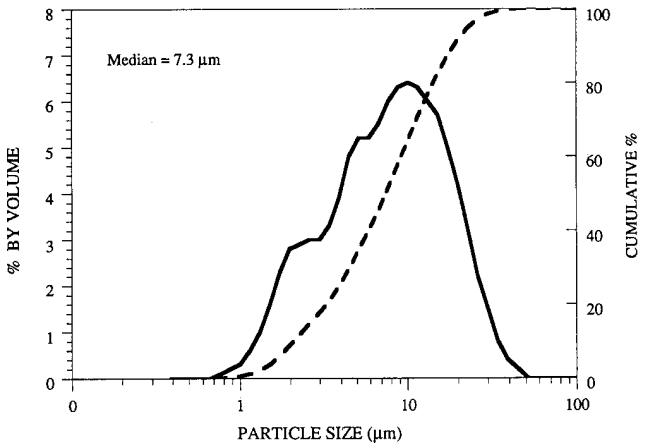

Figure 6. Initial dispersed particle size distribution of sediment sample from Mission Bay. Solid curve is the percent volume and the dashed curve represents cumulative percent finer.

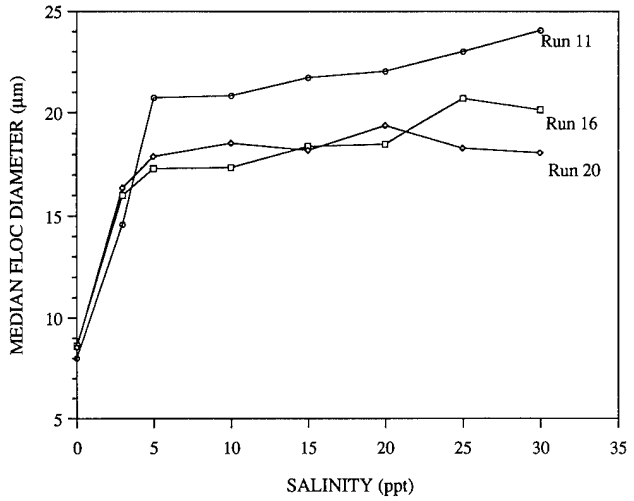

Figure 7. Variations in median floc diameter due to salinity effects.

$10^{-6}M$ compared to only $10^{-8}M$ found in seawater; however, the conductance of H^+ ions is no more than 10 times greater than that of Na^+ ions, whose abundance is 4 to 5 orders of magnitude higher than the H^+ ions in the NaCl solution. Thus the conductance would vary by only 0.01 to 0.1% owing to the difference in H^+ ion concentration between seawater and an artificial NaCl solution. The other source of variance might arise from the *p*H dependent ratio of carbonate to bicarbonate ions in seawater. However these ions amount to only 0.5% of the total sea salts. Although the ratio of these species might vary as much as 30% over the *p*H range between seawater and NaCl solutions in deionized water, these variations would change the total conductance by only 0.15%. Hence the abundance of Na^+ ions overwhelms all the other possible sources of conductance in both natural seawater and artificial NaCl solutions at estuarine salinity levels of 5×10^{-2} to $5 \times 10^{-1}\,M$. These arguments are supported by several investigators who have found that *p*H effects are apparent at salt concentrations several orders of magnitude less than this range. In particular: (1) *Williams and Williams* [1982] show little variation of yield stress with *p*H at electrolyte concentrations of 10^{-2}, 10^{-3}, and $10^{-4}\,M$ NaCl. The variation becomes even smaller at progressively higher NaCl concentrations. (2) *James and Williams* [1982] show that the relationship between shear stress and shear rate is very similar for *p*H 6, 7, and 8. These measurements were conducted at 0.1 *M* NaCl concentrations. James and Williams also measured electrophoretic mobilities of a quartz mineral and sodium-kaolinite at *p*H 6, 7, and 8. Their results show negligible changes of electrophoretic mobility with *p*H. (3) *Rand and*

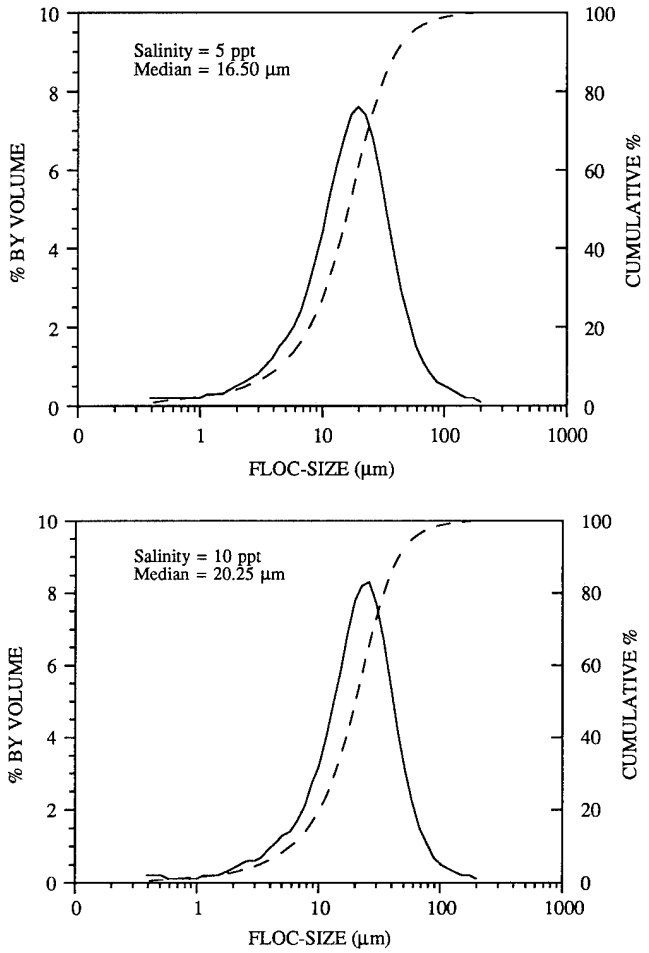

Figure 8a. Floc- size distributions at salinities of 5 and 10 ppt.

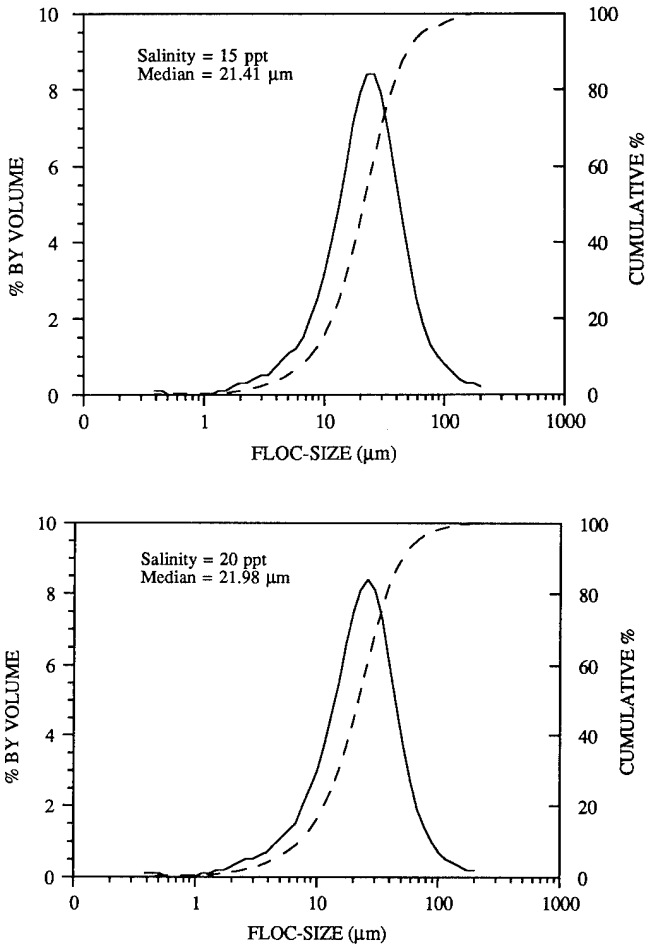

Figure 8b. Floc- size distributions at salinities of 15 and 20 ppt.

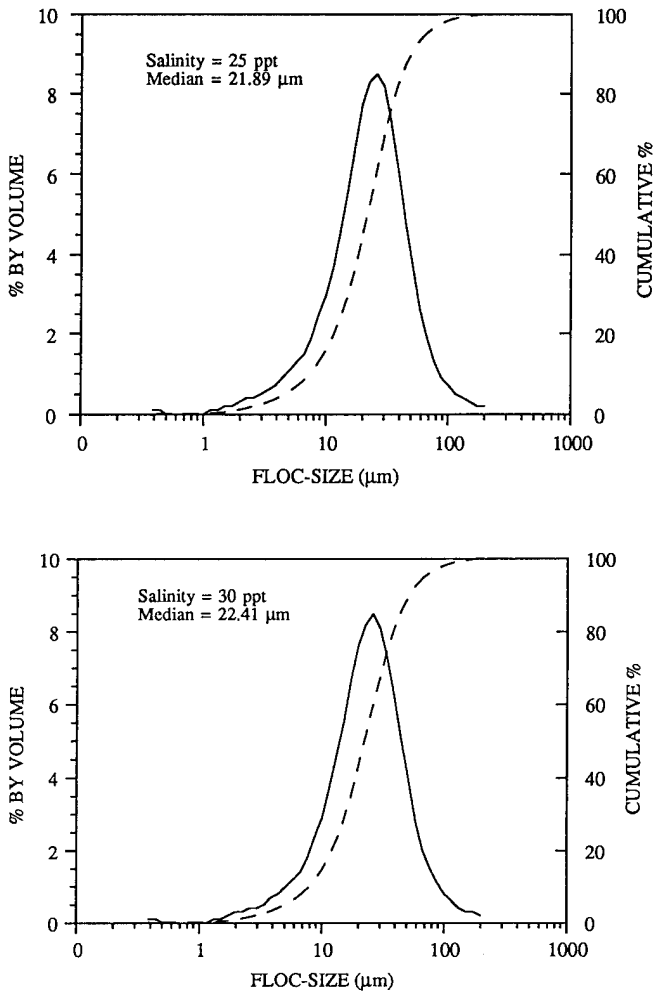

Figure 8c. Floc- size distributions at salinities of 25 and 30 ppt.

Melton [1977] describe the effects of *p*H and NaCl on rheological properties in sodium-kaolinite suspensions. They show that above an electrolyte concentration of 0.12 *M*, the *p*H value of the suspension becomes unimportant.

Theory

We shall explore the hypothesis that the shear stress depends primarily on the viscous and electrokinetic properties of the fluid-sediment suspension. For small particles in a laminar flow where the inertial effects are negligible compared to the viscous forces, the equation of motion is given by [*Booth*, 1950]:

$$\nabla.\tau - \rho_e \nabla\psi - J \times B = 0$$

Relative to the Navier-Stokes equation, the new terms are the electroviscous term ($\rho_e \nabla\psi$) and the electromagnetic term ($J \times B$). J is the electric current density, measured by knowing the charge density of the particles in suspension; B is the induced magnetic field calculated by Ampere's Law; ρ_e is the charge density of the suspension; and ψ is the electric potential taken equal to ζ, the zeta potential. The zeta potential is the electric potential across the shearing plane between the bulk liquid and the envelope of water which moves with the particle. Since the position of this shearing plane is not known, the zeta potential represents the electric potential at a distance from the outer surface of the double layer (we take $\nabla\psi = \nabla\zeta$). *Booth* [1950] and *Russel* [1976] treated the electroviscous effects in the asymptotic limit of low surface potentials and large double layers and concluded that electrostatic interactions dominate the stress generated by the distortion of ions in the double layer.

We consider the motion of fluid rotating in the space between two coaxial cylinders. The outer cylinder is fixed and inner has a torque applied to it which causes it to rotate with angular velocity, ω. In this case, the steady state equation of motion may be written as

$$\frac{d\tau}{dr} + \frac{2\tau}{r} - \rho_e \frac{d\zeta}{dr} - J_r B_z = 0 \qquad (4)$$

The double layer constitutes the charge on the particle as well as the counterions or the exchangeable ions. The parameters associated with the electroviscous effects are κ^{-1}, the Debye-Huckel length or the thickness of the double layer, and the zeta potential, ζ.

When particles are irregular-shaped, the electrophoretic mobility of particles can be used to give a reasonable description of the zeta- potential [*Leong and Boger*, 1990]. The electrophoretic mobility is converted to the zeta potential using the Helmholtz-Smoluchowski equation:

$$u_e = \frac{u}{E} = \frac{\zeta \varepsilon \varepsilon_o}{\mu} \qquad (5)$$

From (5), we get

$$\zeta = \frac{\mu}{\varepsilon \varepsilon_o}\left(\frac{u}{E}\right) \qquad (6)$$

where u_e is the electrophoretic mobility, equal to u/E, μ is the viscosity of the fluid, ε_o is the permittivity of free space equal to $8.85 \times 10^{-12}\,CV^{-1}m^{-1}$ and ε is the dielectric constant of the medium. It is assumed that the charge is uniformly distributed over the surface of the particle. It is recognized that the computation of zeta potential from the electrophoretic mobilities is subject to several corrections. Recent developments in the calculation of zeta potential from electrophoretic mobilities are given by *Wiersema et al.* [1966] and *O'Brien and White* [1978]. However, these techniques are very cumbersome to use. The calculation of zeta potential using the methods of *Wiersema et al.* [1966] requires preparation of a number of graphs to obtain various functions. Also, the final results reduce to the Smoluchowski equation for very large values of κa. In the present study, we use high concentrations of salt or electrolyte, hence we have very large values of κa. Therefore we shall simply use the Smoluchowski equation, (6), to calculate zeta potentials from the electrophoretic mobilities.

The velocity of fluid inside a coaxial cylinder is given by [*Tritton*, 1977]

$$u = \frac{\omega r_b^2 (r_c^2 - r^2)}{r\,(r_c^2 - r_b^2)} \qquad (7)$$

where r_b is the radius of the inner cylinder or the spindle, r_c is the radius of the outer cylinder, and ω is the angular velocity of the inner cylinder.

Assuming that the ions move with the same speed as the fluid in the viscometer, we have

$$u_e = \frac{u}{E} = \frac{\omega r_b^2 (r_c^2 - r^2)}{Er\,(r_c^2 - r_b^2)} \tag{8}$$

Substituting (8) in (6):

$$\zeta = \frac{\mu r_b^2}{\varepsilon\varepsilon_0}\left(\frac{\omega}{E}\right)\frac{(r_c^2 - r^2)}{(r_c^2 - r_b^2)r} \tag{9}$$

Now $\nabla\psi = \nabla\zeta = d\zeta/dr$ is given by

$$\frac{d\zeta}{dr} = -\frac{\mu r_b^2}{(r_c^2 - r_b^2)\varepsilon\varepsilon_0}\left(\frac{\omega}{E}\right)\frac{(r_c^2 + r^2)}{r^2} \tag{10}$$

The total charge on the surface of the particle (considering the double layer around a spherical particle) is given by the Gouy-Chapman theory [see *Hunter*, 1981] as

$$Q = (4\pi\varepsilon\varepsilon_0)\, a(1 + \kappa a)\zeta \tag{11}$$

where a is the radius of the spherical particle and κ^{-1} is the Debye-Huckel length or the thickness of the double layer, defined as

$$\kappa^{-1} = \sqrt{\frac{\varepsilon\varepsilon_0 KT}{ce^2\nu^2}} \tag{12}$$

where c is the molar concentration of salts in the suspension, e is the electric charge, K is the Boltzmann constant, T is the absolute temperature, and ν is the valency of counterions. Since we consider NaCl to be the only salt present in the suspension, ν is equal to one.

The total volumetric charge, ρ_e, is obtained by multiplying the total charge on the particle by the number of particles per unit volume. Therefore, ρ_e is equal to

$$\rho_e = Qn = (4\pi\varepsilon\varepsilon_0)a(1 + \kappa a)\zeta n$$

where n is the number of particles per unit volume. Substituting the value of ζ from (9)

$$\rho_e = 4\pi a\,(1 + \kappa a)\, n\, \mu r_b^2 \left(\frac{\omega}{E}\right)\frac{(r_c^2 - r^2)}{(r_c^2 - r_b^2)r} \tag{13}$$

We use (10) and (13) to solve (4) with the boundary condition that $\tau = \tau_o$ at $r = r_b$, where r_b is the radius of the spindle of the viscometer and τ_o is the shear stress for zero salinity at radius r_b. Employing this boundary condition, (4) is solved for τ and the solution is

$$\tau = \frac{a(1+\kappa a)\alpha\mu^2 u_e^2 n}{\varepsilon r^2}\left[r_c^4 \ln\frac{r_b}{r} + \frac{r^4}{4}\left(1 - \frac{r_b^4}{r^4}\right)\right] + \frac{\beta r}{3}\left[1 - \frac{r_b^3}{r^3}\right] + \tau_o\frac{r_b^2}{r^2} \tag{14}$$

where α includes constants and is defined as

$$\alpha = \frac{4\pi r_b^2}{(r_c^2 - r_b^2)^2\varepsilon_0}$$

and β is defined as

$$\beta = \frac{4\pi r_b^4\omega^2\rho_e^2\mu'}{(r_c - r_b)(r_b + r_c)^4}\left[r_c^2 - \frac{1}{3}(r_b^2 + r_c^2 + r_b r_c)\right]^2$$

where μ' is the magnetic permeability and L is the length of the outer cylinder of the viscometer.

Because of the small annular space in the coaxial viscometer and the stress transfer to the outer cylinder, we solve for the average shear stress across the radii r_b to r_c as given by

$$\tau_{avg} = \frac{a(1+\kappa a)\alpha\alpha_1\mu^2 u_e^2 n}{\varepsilon} + \beta\beta_1 + \tau_o\frac{r_b}{r_c} \tag{15}$$

where α_1 and β_1 are given by

$$\alpha_1 = \frac{r_c^3}{r_b(r_c - r_b)}\left[r_c \ln\frac{r_b}{r_c} - r_b + r_c\right] + \frac{1}{4}\left[\frac{r_c^3 - r_b^3}{3(r_c - r_b)} - \frac{r_b^3}{r_c}\right]$$

$$\beta_1 = \frac{1}{3\,(r_c - r_b)}\left[\frac{(r_c^2 - r_b^2)}{6} + r_b^3\,(r_c^{-1} - r_b^{-1})\right]$$

The stress generated by the magnetic field terms is found to be on the order of 10^{-15} dyn/cm^2, which is negligible compared to 10^{-1} to 1 dyn/cm^2 generated by the electrical interactions. Hence we conclude that the effects of induced magnetic field on the shear stress are negligible.

Equation (12) shows that κ^{-1}, the thickness of the double layer, will decrease with increasing c, the salt concentration. As c increases, there are greater numbers of Na^+ ions available as exchangeable ions. The water molecules around the negatively charged sediment particle are displaced and the electric double layer is compressed. The compression of the double layer causes a fall in the zeta potential owing to the displacement of ions. This distortion of ions in the double layer gives rise to stresses in the suspension which contribute to the increase in the shear stress of the fluid-sediment suspension.

Figure 9 shows the values of shear stress obtained from the experimental data as compared to those predicted by (15) using

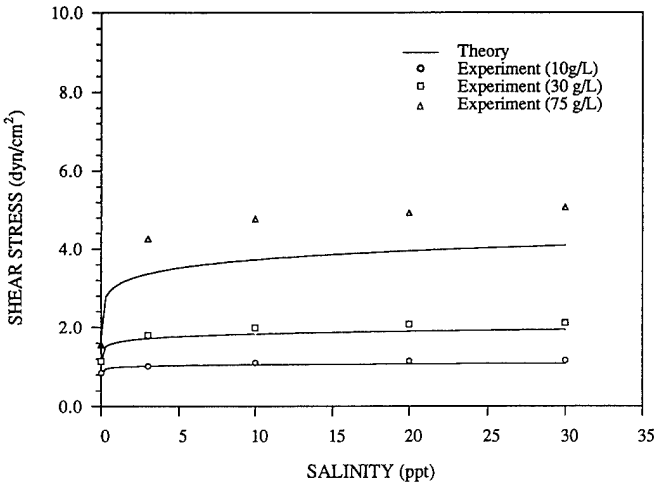

Figure 9. Comparison of shear stress values obtained from experiments and from equation (15).

the zeta potential computed from the polynomial fit in Figure 5. There is reasonable agreement between the data and (15) at low-sediment concentrations. As the sediment concentration increases, the model equation deviates away from the data but still shows a similar trend. This deviation is probably due to the approximation used in employing Gouy-Chapman theories, which are derived for dilute particle concentrations and noninteracting double layers. The model underestimates the shear stress of actual data at sediment concentrations above 30 to 40 g/L. This is expected since the model does not include shear stresses produced because of friction and collisions between particles as the particle concentration increases. Although this model provides a relationship between the salinity variations and the shear stress, which is consistent with our experimental data, it does not account for the effects of interparticle friction and floc breaking due to collisions of flocs, which one would expect to be increasingly important at higher-sediment concentrations.

Conclusions

It was observed that the shear stress increased exponentially with increasing sediment concentration. The shear stress increased logarithmically with increasing salinity. The growth of shear stress was rapid in the lower-salinity range (0-3 ppt), while the increase was gradual in the higher-salinity range (3-30 ppt). There was a 15-20% increase in shear stress as the salinity increased from 3 to 30 ppt.

The zeta potential measurements show a steady decline of the zeta potential with the increase in salinity. This result is comparable to the results obtained by previous investigators for fine sediments.

The floc- size studies showed that there was a systematic increase in the median floc diameters until salinities exceeded 25 ppt. The growth in floc- size paralleled the increase in shear stress observed for increasing salinities up to 25 ppt. The floc- size measurements may not have been accurate for large flocs formed above 25 ppt owing to instrument limitations. Therefore no quantified relationships between floc- size and salinity were obtained for high salinities.

A quantitative link between the basic surface properties of the particles and the macroscopic rheology of the fluid-sediment suspension is demonstrated. Using the classical equations of Gouy-Chapman and Smoluchowski, a simple model is developed which emphasizes the importance of the electrokinteic behavior of the sediment particles on the shear stress of the suspension. The model predicts the shear stress as a function of salt concentration, sediment concentration, and the charge density of the particles. The induced magnetic field strengths of the moving charged particles were found to make a negligible contribution to the total shear stress. The major approximation used is the assumption of dilute particle concentrations in Gouy-Chapman theories. The calculations indicate that the above assumption leads to a qualitative and quantitative agreement with the actual suspension behavior based on measured variations in zeta potential as a function of salinity. The agreement between the theory and data is best at low-sediment concentrations where the assumptions of Gouy-Chapman theories are met, with increasing deviation at high-sediment concentrations. Inclusion of particle collisions at high-particle concentration may improve the quantitative predictions.

Acknowledgments. The project was supported in part by ONR grant N00014-89-J-1117 and in part by the Government of Pakistan through a fellowship awarded to the first author. The laser diffraction particle size analyzer was leased by the Horiba Instruments Inc. on a special agreement. We thank Joe Wasyl, Edward Trevino, and David Skelly for sample collection.

References

Aijaz, S., The dependence of dynamic shear stress on NaCl ionic strength in cohesive sediment suspensions, Masters thesis, 79 pp., Univ. of Calif. San Diego, La Jolla, 1989.

Bennett, R.H., N.R. O'Brien, and M.H. Hulbert, Determinants of clay microfabric signatures: Processes and mechanisms, in *Microstructure of Fine Grained Sediments, From Mud to Shale*, edited by R.H. Benette, W.R. Bryant, and M.H. Hulbert, pp. 5-32, Springer-Verlag, New York, 1991.

Booth, F., Electroviscous effect for suspension of solid spherical particles, *Proc., R. Soc., London, A, 203* , 533-551, 1950.

Bryant, R., A.E. James, and D.J.A. Williams, Rheology of cohesive suspensions, in *Industrialized Embayments and Their Environmental Problems*, edited by M.B. Collins, pp. 279-287, Pergamon, New York, 1980.

Burban, P-Y., W. Lick, and J. Lick, Flocculation of fine grained sediments in estuarine waters, *J. Geophys. Res., 94,* 8323-8330, 1989.

Butters, G., and A.L. Wheatley, Experience with the Malvern ST1800 laser diffraction particle size analyzer, in *Particle Size Analysis,* edited by S.N. Wood and T. Allen, pp. 425-436, Wiley-Heden, Chichester, U.K, 1982.

Das, M.M., Study of Bingham shear strength of a deep marine sediment by capillary viscometer, in A Literature Review on Erosion and Deposition of Sediment Near Structures in the Ocean, edited by H.A. Einstein and R.L. Wiegel, *Rep. HEL-21-6,* pp. 2-1-2-35, Hydraul. Eng. Lab., Coll. of Eng., Univ. of Calif., Berkeley, 1970.

Dyer, K.R., *Coastal and Estuarine Sediment Dynamics*, 342 pp., John Wiley, New York, 1986.

Edzwald, J.K., J.B. Church, and C.R. O' Melia, Coagulation in estuaries, *Environ. Sci. Technol., 8,* 58-63, 1974.

Einstein, H.A., and R.B. Krone, Experiments to determine the modes of cohesive sediment transport in salt water, *J. Geophys. Res., 67,* 1451-1461, 1962.

Eirich, F.R., *Rheology, Theory and Applications,* vol. 3, 680 pp., Academic, San Diego, Calif., 1960.

Faas, R.W., A portable rotational viscometer for field and laboratory analysis, *J. Coastal Res., 6,* 735-738, 1990.

Gibbs, R.J., Coagulation rates of clay minerals and natural sediments, *J. Sediment. Petrol., 53,* 1193-1203, 1983.

Gripenberg, S., A study of sediments of the Baltic and the adjoining seas, *Fennia, 60,* 1-231, 1934.

Heugen, P., and M.A. Tung, Rheograms for Power-law fluids using coaxial cylinder Viscometers and a Template method, *Can. Inst. Food Sci.Technol. J., 9,* 98-104, 1976.

Hunter, R.J., *Zeta Potentials in Colloid Science*, 386 pp., Academic, San Diego, Calif., 1981.

Hunter, R.J., The flow behavior of coagulated colloidal dispersions, *Adv. Colloid Interface Sci., 17,* 197-211, 1982.

Hunter, K.A., and P.S. Liss, The surface charge of suspended particles in estuarine and coastal waters, *Nature, 282,* 823-825, 1979.

James, A.E., and D.J.A. Williams, Flocculation and rheology of kaolinite/quartz suspensions, *Rheol. Acta, 21,* 176-183, 1982.

Jackson, M.L., Soil Chemical Analysis-Advanced Course, 2nd ed., Dept. of Soil Sci., Univ. of Wisc., Madison, 1969.

Jenkins, S.A., and J.A. Bailard, Anti-sedimentation system for harbors, *World Wide Shipping, 52,* 70-75, 1989.

Jenkins, S.A., and J. Wasyl, Resuspension of estuarine sediments by tethered wings, *J. Coastal Res., 6,* 961-980, 1990.

Jenkins, S.A., S. Aijaz, and J. Wasyl, Transport of fine sediments by hydrostatic jets, in *Nearshore and Estuarine Cohesive Sediment Transport, Coastal Estuarine Stud.*, vol. 42, edited by A.J. Mehta, pp.331-347, AGU, Washington, D.C., 1993.

Krone, R.B., Flume studies the transport of sediments in estuarial shoaling processes, final rep., Hydraul. Eng. Lab. and Sanit. Eng. Res. Lab., Univ. of Calif., Berkeley, 1962.

Krone, R.B., The significance of aggregate properties to transport processes, in *Estuarine Cohesive Sediment Dynamics,* edited by A.J. Mehta, pp. 66-84, Springer-Verlag, New York, 1984.

Lambermont, J., and G. Lebon, Erosion of cohesive soils, *J. Hydraul. Res., 16,* 27-44, 1978.

Leong, Y., and D.V. Boger, Surface chemistry effects on concentrated suspensions, *J. Colloid Interface Sci., 136,* 249-258, 1990.

Meade, R.H., Transport and deposition of sediments in estuaries, *Mem. Geol. Soc. Am., 133,* 91-120, 1972.

Mehta, A.J., On estuarine cohesive sediment suspension behavior, *J. Geophys. Res., 94,* 14,303-14,314 , 1989.

McCave, I.N., R.J. Bryant, H.F. Cook, and C.A. Coughanowr, Evaluation of a laser diffraction size analyzer for use with natural sediments, *J. Sediment. Petrol., 56,* 561-564, 1986.

O'Brien, R.W., and L.R. White, Electrophoretic mobility of a spherical colloidal partocle, *J. Chem. Soc. Faraday Trans 2, 74,* 1607-1626, 1978.

Pierce, J.W., and F.R. Siegel, Particulate material suspended in estuarine and oceanic waters, in Scanning Electron Microscopy, I, pp. 555-562, SEM Inc., AMF O' Hare, Ill., 1979.

Partheniades, D., Erosion and deposition of cohesive soils, *J. Hydraul. Div., Am. Soc. Civ. Eng., HY1,* 105-139, 1965.

Rand, B., and I.E. Melton, Particle interactions in aqueous kaolinite suspensions, *J. Colloid Interface Sci., 60,* 308-320, 1977.

Rashid, M.A., *Geochemistry of Marine Humic Compounds,* 300 pp., Springer-Verlag, New York, 1985.

Rashid, M.A., D.E. Buckley, and K.R. Robertson, Interactions of a marine humic acid with clay minerals and a natural sediment, *Geoderma, 8,* 11-27, 1972.

Rosen, M.R., A rheogram template for Power-law fluids, rapid rheological characterization in a coaxial cylinder, *J. Colloid Interface Sci., 39,* 413-417, 1972.

Russel, W.B., Lower-shear limit of the secondary electroviscous effect, *J. Colloid Interface Sci., 55,* 590-604, 1976.

Singer, J.G., J.B. Anderson, M.T. Ledbetter, I.N. McCave, K.P.N. Johns, and R. Wright, An assessment of analytical techniques for the size analysis of fine grained sediments, *J. Sediment. Petrol., 58,* 534-543, 1988.

Stumm, W., and J.J. Morgan, *Aquatic Chemistry,* 780 pp., John Wiley, New York, 1981.

Tritton, D.J., *Physical Fluid Dynamics,* 362 pp., Van Nostrand Reinhold, New York, 1977.

Van Olphen, H., *An Introduction to Clay Colloid Chemistry,* 318 pp., John Wiley, New York, 1977.

Van Wazer, J. R., J. W. Lyons, K. Y. Kim, and R. E. Colwell, *Viscosity and Flow Measurements: A Laboratory Handbook of Rheology,* 406 pp., John Wiley, New York, 1963.

Whitehouse, U.G., l.M. Jefferey, and J.D. Debbrecht, Differential settling tendencies of clay minerals in saline waters, *Clays and Clay Minerals, 7,* 1-79, 1960.

Wiersema, P.H., A.L. Loeb, and J.T.G. Overbeek, Calculation of electrophoretic mobility of a spherical colloid particle, *J. Colloid Interface Sci., 22,* 78-99, 1966.

Williams, D.J.A., and K.P. Williams, Colloid stability and rheology of kaolinite suspensions, *Trans. Bri. Ceram., Soc., 81,* 78-83, 1982.

Williams, D.J.A, and K.P. Williams, Electrophoresis and zeta potential of kaolinite, *J. Colloid Interface Sci., 65,* 79-87, 1978.

Williams, D.J.A., Rheology of cohesive suspensions in *Estuarine Cohesive Sediment Dynamics,* edited by A.J. Mehta, pp.110-125, Springer-Verlag, New York, 1986.

Williams, D.J.A. and P.R. Williams, Rheology of concentrated cohesive sediments, *J. Coastal Res., SI 5,* 165-173, 1989.

Zabawa, C.R., Microstructure of agglomerated suspended sediments in Northern Chesapeake Bay Estuary, *Science, 202,* 49-50, 1978.

S. Aijaz and S.A. Jenkins, Scripps Institution of Oceanography, 9500 Gilamn Drive, La Jolla, CA 92093-0209.

(Received March 8, 1993; revised November 5, 1993;
accepted December 6, 1993.)

APPENDIX B

FLUID-SEDIMENT INTERACTIONS AND DYNAMIC SHEAR STRESS IN FINE SEDIMENT SUSPENSIONS

Saima Aijaz & Scott A. Jenkins

Powders & Grains 93, Thornton (ed.) © 1993 Balkema, Rotterdam, ISBN 90 5410 323 X

Fluid-sediment interactions and dynamic shear stress in fine sediment suspensions

Saima Aijaz & Scott A.Jenkins
Scripps Institution of Oceanography, University of California, San Diego, Calif., USA

ABSTRACT: The effects of flocculation on the rheology of fine sediment suspensions are inverstigated. It was found that the dynamic shear stress increases with the increasing sediment concentration and increases logarithmically by increasing the salinity of the suspension. The salinity dependence of the dynamic shear stress was correlated with changes in floc-size. These results reflect the dominant influence of fluid-sediment interactions on the flocculation behavior of the suspension. An analytic model predicting shear stress as a function of electrokinetic properties of the fine sediment suspension is developed.

1 INTRODUCTION

The dynamic shear stress induced in a fine cohesive sediment suspension is commonly believed to result from friction due to the relative motion and interaction of the fluid and the sediment particles (Lambermont & Lebon 1978). It has also been attributed to the stress required to break the bonds within floc aggregates of sediment particles during shearing (Krone 1962). This paper reports the behavior of dynamic shear stress of naturally occuring sediment suspensions as a function of fluid-sediment properties that affect the flocculation process. Elevated dynamic shear stress measurements are believed to result from: 1) fluid-sediment interactions due to electrochemical processes; 2) interparticle friction as complex floc aggregates collide and rub together.

2 EXPERIMENTAL RESULTS & DISCUSSION

The sediment samples were collected from Mission Bay, San Diego. The predominant minerals present in the sediment were montmorillonite, illite and kaolinite. The shear stress was measured at varying salinities and sediment concentrations using a Brookfield Viscometer. Salinity was represented by NaCl in parts by thousand (ppt). The shear stress rises exponentially with the rise in sediment concentration. The relationship between salinity and shear stress for natural sediments is shown in Fig.1. As the salinity is increased from 0 to 3 ppt, there is a sharp increase in the rise in shear stress followed by a gradual increase beyond 3 ppt. This indicates that flocculation is critical at low salinities. The floc-size measurements were carried out using a Laser Sizer which causes minimum disturbance to flocs. The floc-size results indicate an increase in the median diameter of the flocs with the increase in salinity (Fig.2). The growth in floc-size paralleled the increase in shear stress observed for increased salinities. The study of surface chemistry consisted of determining the zeta potential which gives a measure of the surface charge density of the particles (Van Olphen 1977). It is computed from the electrophoretic mobility (motion of particles under an applied electric field). The electrophoretic mobility (E.M) of the particles was measured by the standard method of microelectrophoresis. It is observed that the electrophoretic mobility of sediment particles steadily declines with increasing salinity. Fig.3. shows the comparison of data from the present study to that of Hunter & Liss (1979). As the salt concentration, increases, there are greater numbers of Na^+ ions available as exchangeable ions. The water molecules around the negatively charged sediment particle are displaced and the electric double layer is compressed. The compression of the double layer causes a fall in the zeta-potential due to the displacement of ions. This distortion of ions in the double-layer gives rise to stresses in the suspension which contributes to the increase in dynamic shear stress of the sediment suspension.

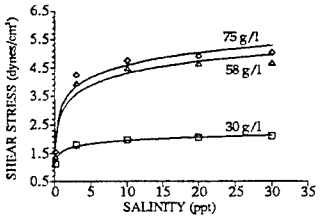

Fig.1. Effect of salinity on shear stress

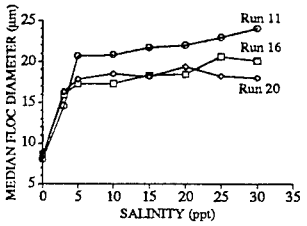

Fig.2. Effect of salinity on median floc diameter

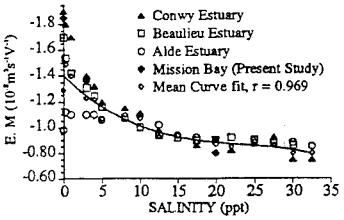

Fig.3. E.M of particles as function of salinity

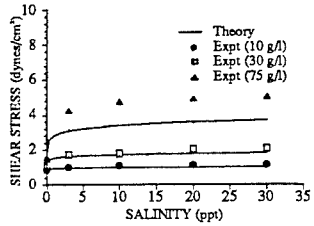

Fig.4. Comparison of model with experimental data

3 MODEL

A simple analytic model based on the electroviscous properties of the suspension is developed. The parameters associated with the electroviscous effects are κ^{-1}, the Debye-Huckel length or the thickness of the double layer, and the zeta-potential. The model incorporates the Gouy-Chapman theory of the electric double layer and the Smoluchowski theory for the electrokinetics of fluid-sediment interactions (see Kruyt (1952) for a review of these theories). The details of the formulation of the model are given in Aijaz (1993) and Aijaz & Jenkins (1992). The model predicts shear stress as a function of the electrokinetic and physical properties of the fluid-mud suspension as follows:

$$\tau = \tau_0 \frac{r_b}{r_c} + \frac{(1+\kappa a)\alpha\mu^2 u_e^2 N/a^2}{\varepsilon} \qquad (1)$$

where u_e is the electrophoretic mobility; μ is the viscosity of the fluid; ε is the dielectric constant of the medium; a is the particle radius; N is the volumetric concentration of the sediment suspension; τ_0 is the measured shear stress at zero salinity; r_c is the radius of outer cylinder of the Viscometer; r_b is the radius of the inner cylinder; α is a constant which includes the Boltzmann constant, temperature, permittivity in vaccum and geometry of the Viscometer. The main limitation of the model is that it is valid only for non-aggregating particles in dilute suspensions. Fig.4. shows values of shear stress obtained from the experimental data as compared against those predicted by equation (1). There is reasonable agreement between the data and equation (1) at low sediment concentrations. As the sediment concentration increases, equation (1) deviates away from the data but still shows a similar trend. This deviation is probably due to the approximation used in employing Gouy-Chapman theories which are derived for dilute particle concentrations. Although, this model provides a relationship between the salinity variations and the shear stress which is consistent with our experimental data, it does not account for the effects of interparticle friction and floc breaking due to collisions of flocs, which one would expect to be increasingly important at higher sediment concentrations.

REFERENCES

Aijaz,S. & S.A.Jenkins 1992. On the electro-kinetics of dynamic shear stress in fluid-mud suspensions. *J.Geophys.Res.* submitted.

Aijaz,S. 1993. Dynamic shear stress in fluid-mud suspensions. Ph.D Thesis, University of California, San Diego, USA.

Hunter, K.A. & P.S.Liss 1979. The surface charge of suspended particles in estuarine and coastal waters. *Nature* 282: 823-825.

Krone, R.B. 1962. Final Report, Hydraulic Engg. Lab. and Sanitary Engg. Res. Lab., Univ. Calif., Berkeley.

Kruyt, H.R. 1952. *Colloid Science, vol 1.* Amsterdam: Elsevier.

Lambermont, J.& G. Lebon 1978. Erosion of cohsive soils. *J.Hydraul. Res.* 16: 27-44.

Van Olphen, H. 1977. *An Introduction to Clay Colloid Chemistry.* New York: John Wiley & Sons.

APPENDIX C

DYNAMICS OF SHEARING IN FLOCCULATING FINE SEDIMENT SUSPENSIONS

Saima Aijaz & Scott A. Jenkins

APPENDIX D

TRANSPORT OF FINE SEDIMENTS BY HYDROSTATIC JETS

Scott A. Jenkins, Saima Aijaz and Douglas Inman

Makromol. Chem., Macromol. Symp. **76,** *89-93 (1993)*

DYNAMICS OF SHEARING IN FLOCCULATING FINE SEDIMENT SUSPENSIONS

Saima Aijaz* & Scott A. Jenkins

Scripps Institution of Oceanography, University of California, San Diego
La Jolla CA 92037-0209, USA

Abstract: The variability of rheological properties in cohesive sediment suspensions are studied and related to the flocculation process. It was found that the steady state shear stress increases exponentially with increasing sediment concentration and increases logarithmically by increasing the salinity of the suspension. The salinity dependence of the shear stress was correlated with changes in the floc-size. These results reflect the dominant influence of fluid-sediment interactions on the flocculation behavior of the suspension. An analytic model predicting shear stress as a function of the physical and electrochemical properties of the fine sediment suspension is developed.

INTRODUCTION

The steady state shear stress induced in a fine cohesive sediment suspension is commonly believed to result from friction due to the relative motion and interaction of the fluid and the sediment particles in a time invariant flow (Ref.1). It has also been attributed to the stress required to break the bonds within aggregates of sediment particles during shearing (Ref.2). Unlike coarse sediments, the fine sediments are not individual units but stick together to form flocs. These flocs may further combine as a result of turbulent shear or sticky organic matter to form floc aggregates or floc networks (Ref.3). Previous studies on flocculation (Ref.4) and rheology (Refs.5,6) of fine sediment suspensions have been done either on pure clay minerals or on colloidal suspensions. This paper reports the shear stress behavior of naturally occurring sediment suspensions as a function of fluid-sediment properties that affect the flocculation process. Elevated shear stress measurements are believed to result from 1) fluid-sediment interactions due to electro-chemical processes, 2) stress transfer through the fluid as geometrically complex floc-networks entrain more fluid, 3) interparticle friction as these complex floc-networks collide and rub together, 4) release of energy due to breaking of bonds between floc-networks during shearing. These interfloc bonds are primarily related to sediment mineralogy, salinity and biogenic influences.

EXPERIMENTAL RESULTS & DISCUSSION

The sediment samples were collected from Mission Bay, San Diego. These were composed of 15% clay, 75% silt and 10% sand, with an organic content of 3%. The predominant minerals present in the sediment were montmorillonite, illite and kaolinite. The shear stress was measured by a Brookfield Viscometer equipped with a UL Adapter. The rheology of the sediment suspension is shown in Fig.1. The suspension exhibits shear thinning behavior

 CCC 0258-0322/93/$ 04.00

which suggests the development of floc structure at low shear rates and a progressive breakdown of the structure with increasing shear rates. (Ref.7). The shear stress was then measured at varying salinities and sediment concentrations. Salinity was represented by NaCl in parts per thousand (ppt). Two sets of experiments were conducted. One consisted of analyzing the shear stress behavior of natural sediment sample, and the other measured the shear stress after removing the organic matter from the sediment sample. Both showed similar trends. Fig.2 shows the exponential rise of shear stress with the rise in sediment concentration. Although, this exponential rate is intriguing, it is a well known result (Ref.2). As the number of particles increases, there is greater probability of interparticle collisions resulting in increased floc-formation. These flocs entrain more fluid and cause a growth in the shear stress.

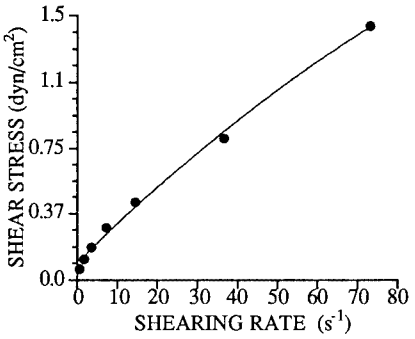

Fig.1. Rheology of fluid-sediment suspension

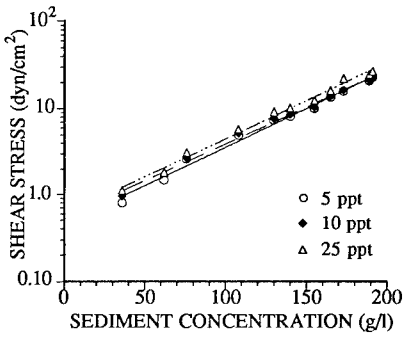

Fig.2. Effect of sediment concentration on shear stress (ppt=parts per thousand)

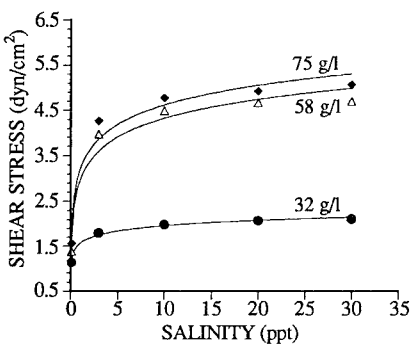

Fig.3. Effect of salinity on shear stress (ppt=parts per thousand)

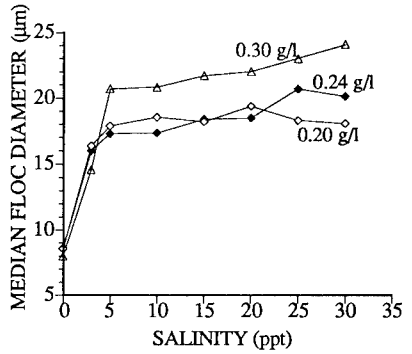

Fig.4. Median floc diameter as a function of salinity (ppt=parts per thousand)

The relationship between salinity and shear stress for natural sediments is shown in Fig.3. Regression analysis by least squares method shows that a logarithmic curve fit to the data

gives a coefficient of correlation as 0.98 for each curve. As the salinity is increased from 0 to 3 ppt, there is a sharp increase in shear stress followed by a gradual increase beyond 3 ppt. This indicates that flocculation is critical at low salinities. Initially, a suspension at rest and at zero salinity would contain dispersed charged particles. As the sediment suspension is sheared in the viscometer, the particles collide due to an increase in the random motion of particles. The increase in Na^+ ions causes a compression of the double layer which allows the particles to bind together into flocs. On continued increase in salinity and continued shearing, the flocs form a network of aggregates. The network bonds are stretched and deformed and once their yield stress is exceeded, the broken fragments snap back to unstrained positions. If shearing continues, then the flocs would break, and cause a decrease in the shear stress. But as the floc-networks become bigger, greater force is required to break the increasing number of floc bonds. Consequently, the shear stress goes on increasing. Thus, the factors responsible for enhancing the shear stress at higher salinities are the geometry and size of the floc network structure and the electrochemistry of the particles that form the floc networks. Accordingly, the floc-size distribution and the surface chemistry of the particles was studied.

The floc-size measurements were carried out using the Laser Diffraction Particle Size Analyzer which causes minimum disturbance to flocs. The floc-size results indicate an increase in the median diameter of the flocs as the salinity increases from zero to 25 ppt (Fig.4). The growth in floc-size paralleled the increase in shear stress observed for increasing salinities up to 25 ppt. Above 25 ppt, the median floc diameter either levels off or decreases slightly. This unexpected result may be caused by instrument limitations.

The study of surface chemistry consisted of determining the zeta potential which gives a measure of the surface charge density of the particles (Ref 8). The zeta potential is the electric potential across the fluid-sediment interface. It is computed from the electrophoretic mobility (motion of particles under an applied electric field) using the Smoluchowski equation, $u_e=\zeta\varepsilon\varepsilon_o/\mu$, where u_e is the electrophoretic mobility, ζ is the zeta potential, μ is the viscosity of the fluid, ε_o is the permittivity in vaccum and ε is the dieclectric constant (dimensionless) of the fluid. The electrophoretic mobility (E.M.) of the particles was measured by the standard method of microelectrophoresis. Measurements were made at varying salinities from 0 to 20 ppt. The instrument did not give stable measurements above 20 ppt. The measured values at these salt concentrations are in close agreement with those of Hunter and Liss (Ref.9). Fig.5 shows the comparison of data from the present study to that of Ref.9. A polynomial curve is fitted to the entire data set. It is observed that the electrophoretic mobility of sediment particles steadily declines with increasing salinity. As the salt concentration, increases, there are greater numbers of Na^+ ions available as exchangeable ions. The water molecules around the negatively charged sediment particle are displaced and the electric double layer is compressed. The compression of the double layer causes a fall in the zeta-potential due to the displacement of ions. This distortion of ions in the double-layer gives

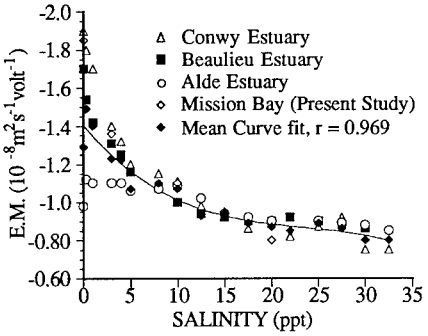

Fig.5. Electrophoretic mobility (E.M.) of particles as a function of salinity

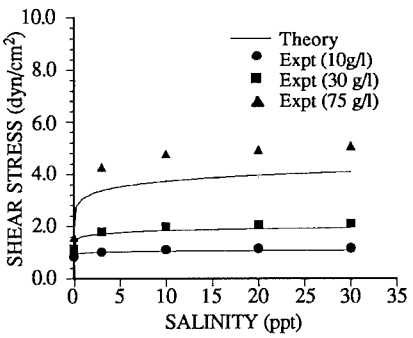

Fig.6. Comparison of experimental data with model

rise to stresses in the suspension which contributes to the increase in the steady state shear stress of the fluid-sediment suspension.

MODEL

A simple analytic model based on the electroviscous properties of the suspension is developed. The model incorporates the Gouy-Chapman theory for computing the charge density of the sediment particle and the Smoluchowski theory for the electrokinetics of fluid-sediment interactions. The details of the formulation of the model are given in Ref.10. The main limitation of the model is that it is valid only for non-aggregating particles in dilute suspensions. It predicts shear stress, τ, as a function of the electrophoretic mobility of particles and the salinity of the suspension as follows:

$$\tau = \frac{4\pi a(1+\kappa a)\mu^2 u_e^2 r_b^2 n\alpha}{\varepsilon\varepsilon_o(r_c^2 - r_b^2)^2} + \tau_o\frac{r_b}{r_c} \qquad (1)$$

where κ is the thickness of the electric double layer, a is the particle radius, τ_o is the measured shear stress at zero salinity, n is the number of particles per unit volume, α is a constant describing the geometry of the viscometer, r_c is the radius of outer cylinder of the viscometer, and r_b is the radius of the inner cylinder. Fig.6 shows values of shear stress obtained from the experimental data as compared against those predicted by equation (1). There is reasonable agreement between the data and equation (1) at low sediment concentrations. As the sediment concentration increases, the model equation deviates away from the data but still shows a similar trend. This deviation is probably due to the approximation used in employing Gouy-Chapman theories which are derived for dilute particle concentrations and non-interacting double-layers. The model underestimates the shear stress of actual data at sediment concentrations above 30 g/l. This is expected because the

model does not include shear stresses produced due to friction and collisions between particles as the particle concentration increases. Although, this model provides a relationship between the salinity variations and the shear stress which is consistent with our experimental data, it does not account for the effects of interparticle friction and floc breaking due to collisions of flocs, which one would expect to be increasingly important at higher sediment concentrations.

REFERENCES

(1) J.Lambermont, G. Lebon, J.Hydraul. Res.,16, 27 (1978)
(2) R.B.Krone, Final Report, Hydraulic Engg. Lab. and Sanitary Engg. Res. Lab., Univ. Calif., Berkeley, (1962)
(3) C.R.Zabawa, Science, 202, 49 (1978)
(4) U.G.Whitehouse, L.M.Jefferey, J.D.Debbrecht, Clays Clay Miner., Proc. 7th Nat. Conf., 7, 1 (1958)
(5) R.J.Hunter, Adv. Colloid Interface Sci., 17, 197 (1982)
(6) D.J.A.Williams, P.R.Williams, J. Colloid Interface Sci., 65, 79 (1978)
(7) A.E James, D.J.A.Williams, Adv. Colloid Interface Sci., 17, 219 (1982)
(8) H.Van Olphen, An Introduction to Clay Colloid Chemistry, John Wiley & Sons, New York (1977)
(9) K.A.Hunter, P.S.Liss, Nature, 282, 823 (1979)
(10) S.Aijaz, S.A.Jenkins, J.Geophys.Res., submitted (1992)

Transport of Fine Sediments by Hydrostatic Jets

Scott A. Jenkins, Saima Aijaz and Joseph Wasyl

Reprinted From *Nearshore and Estuarine Cohesive Sediment Transport*

Ashish J. Mehta (Ed.)

Coastal and Estuarine Studies

Published by the American Geophysical Union

Transport of Fine Sediments by Hydrostatic Jets

Scott A. Jenkins, Saima Aijaz and Joseph Wasyl

The effects of hydrostatic jets (those without propagating horizontal pressure gradients) on the transport and entrainment of fine grain estuarial sediments from the near bottom fluid mud layers are considered. Using mixing length arguments it is proposed that the elevated shear stresses resulting from these jets transport suspended sediment vertically upward across the lutocline, thereby reducing the abundance of suspended sediment directly adjacent to the consolidated bed. Through this entrainment the jets were found to cause reductions in the deposition rates. The extinction of jet-induced bottom stress with increasing distance from the jet was measured on laboratory scales and found to obey a power law over several orders of magnitude. This power law was invoked in a vertical advection-diffusion model to calculate the variation in jet entrainment flux with increasing distance away from the jet discharge nozzle. These calculations were compared with field measurements conducted at three different sites for a variety of jet discharge velocities, diameters and flow rates. When low salinity surface water was pumped through the jets, the entrainment flux at great distances was larger than expected. Consequently, the calculations required the assumption of a reduced cohesive yield stress to match the measured values. This was supported by laboratory viscometer measurements using native suspensions with artificially depressed salinities.

Introduction

Water jets have been employed since the late nineteenth century as a means for agitation dredging. This application requires large amounts of horsepower in order to achieve jet induced shear stresses in excess of the critical erosion stress of consolidated muds. Consequently the jets have only a local effect and require some sort of mobile platform to scour and erode large areas of muddy estuarial waterways. Furthermore significant increases in turbidity result from this practice which ultimately limit its application in environmentally sensitive areas.

In recent years automated jetting systems have been attached to piers and quay walls to resuspend fluid mud before it remains immobile long enough to form partially consolidated mud, see Jenkins, Bailard and Inman (1980), Jenkins

and Bailard (1989), Heinz, Bailard, and Jenkins (1989). In this application the jetting system does not function as a dredging device which must induce erosion. Rather, the jetting system is employed as a depth maintenance device which must merely produce enough bottom stress to exceed the cohesive yield stress of mobile fluid mud in order to effect its resuspension. These automated jetting systems fall into two basic classes; (1) pump based systems; and (2) ducted propeller based systems. The pump based systems consist of a centrally located pump which discharges through a manifold to a line array of fixed bottom mounted jets, see Fig. 1. Control valves at each branch point along the manifold regulate the entire pump discharge sequentially through each jet for a predetermined duty cycle. The bottom mounted jets consist of a convergent nozzle. The operation of the jet system is controlled by a computer which sequences its operations to coincide with early ebbing tide immediately after slack water. When operated on a daily basis only a relatively thin fluid mud layer is reintroduced into the water column, rather than the deposition of an entire season as in the case of agitation dredging.

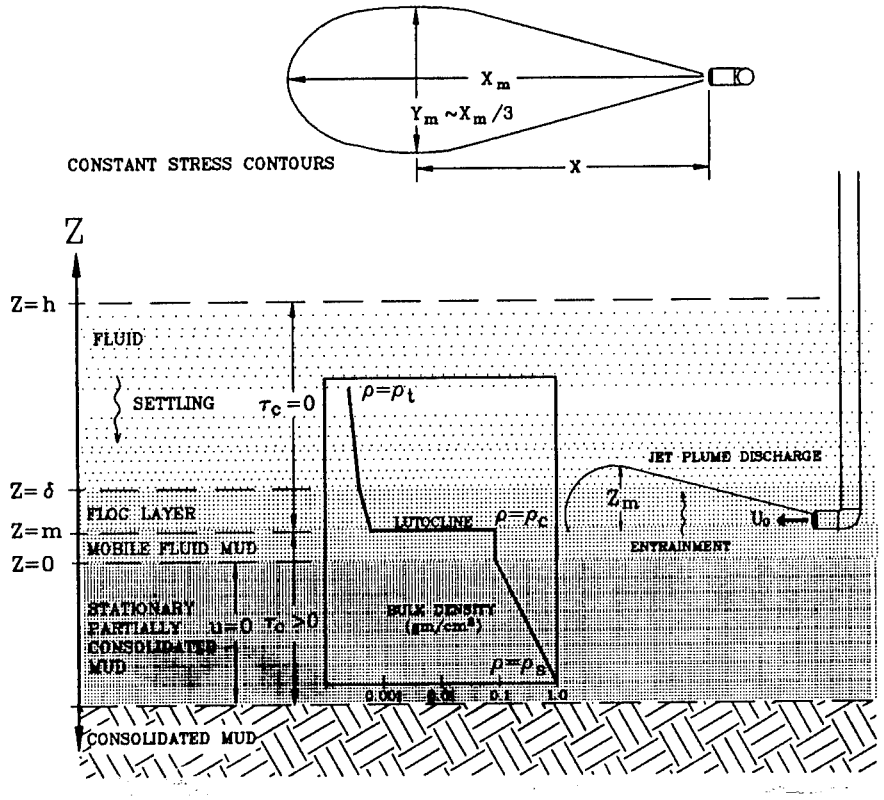

Figure 1. Section view of the pump based jet system at the Port of Grays Harbor, Washington.

The propeller based systems operate in a similar manner, but employ ducted fans rather than centrifugal impellers to drive the jet flow, see Fig. 2. These systems are detailed in Bailard and Jenkins (1990). The propeller is mounted inside a vertically oriented 90° elbow with a horizontal discharge at the bottom. This configuration protects the propeller from bottom debris or slumping mud banks, as commonly found beneath piers and docks. The elbow may be hinged to a frame and articulated with a hydraulic ram to allow the jet to scan through 180° arcs, thereby increasing the area of influence of the jet discharge. Whereas the pump based systems generally produce a high velocity low flow rate jet through a small convergent nozzle, the propeller based system produces a relatively low velocity jet at a very high flow rate. We shall show subsequently that either high velocity or high flow rate jets are capable of elevating bottom stresses sufficiently to exceed the cohesive yield stress of fluid mud and thereby induce resuspension.

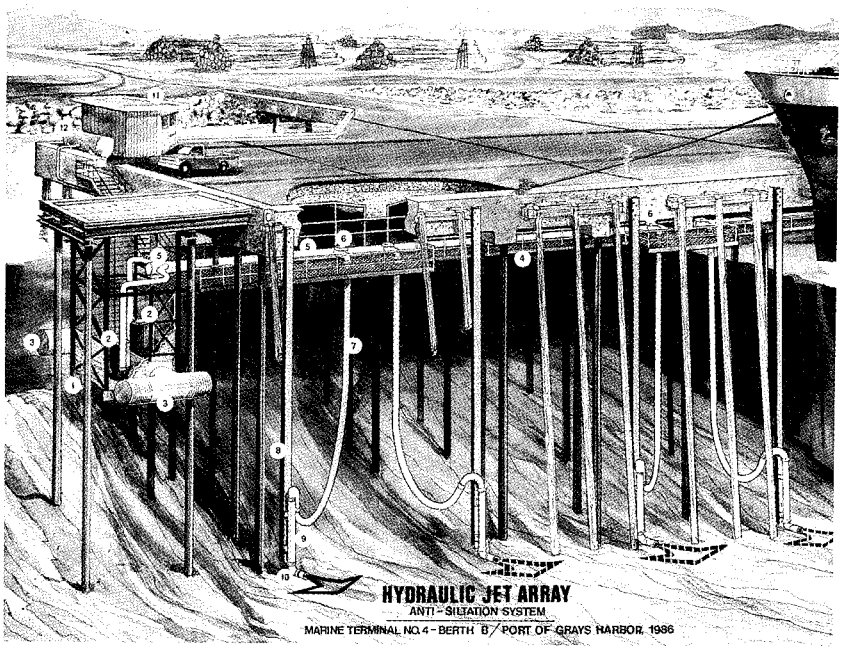

Figure 2. Schematic of the propeller based jet system tested at the Port of Grays Harbor November 1989 - February 1990. Components are indicted as follows: 1) pump chamber; 2) 400 h.p. pump; 3) water intake screens; 4) access catwalk; 5) 24" manifold pipe; 6) butterfly control valve; 7) 12" nozzle supply hose; 8) nozzle guide pile; 9) nozzle support assembly; 10) nozzle - 13,700 g.p.m. output; 11) control house; 12) air tank.

Theory

Consider a jet discharging horizontally across a partially consolidated muddy bottom at z = 0, as shown in Fig. 3. Let the jet diameter at the discharge point be, d, where the centerline axial velocity of the jet discharge is U_0. Above the bottom at z = 0 assume a suspension of uniform particles, each with a settling velocity relative to the fluid, ω_0 and a solid density, $\rho_q = 2.65$ g/cm^3. If the density of the fluid is ρ_f, then the density of the fluid sediment mixture, ρ_m may be written:

$$\rho_m = \rho_q N + (1-N)\rho_F \tag{1}$$

where N is the volume concentration equal to the volume of sediment per volume of the fluid-sediment mixture. The density of the sediment component of this mixture, ρ, is sometimes referred to as the excess density and is defined:

$$\rho = \rho_q N \tag{2}$$

The upper regions of the water column are relatively deficient of suspended sediment, where the density of the sediment component at the free surface, z = h, is $\rho = \rho_t$. Because of settling under the influence of gravity the abundance of suspended sediment begins to increase in the neighborhood of the bottom below z = δ, forming a non-cohesive floc layer as shown in Fig. 3, see Mehta and Partheniades (1975) and Krone (1978). At the bottom of the floc layer, at z = m, there is a rapid increase in bulk density referred to in the recent literature as a lutocline, see Dyer (1985) and Mehta (1989). At or below the lutocline the suspended sediment concentrations are sufficiently high for the fluid sediment mixture to exhibit a non-zero cohesive yield stress, τ_c, and behave therefore as a viscoplastic. Above the lutocline at z = m, the cohesive yield stress vanishes and the fluid sediment mixture behaves as a fluid, i.e. unable to support shear stress at equilibrium. The sediment component density at z = m, where the fluid sediment mixture first begins to exhibit a cohesive yield stress, is $\rho = \rho_c$. The region between the lutocline and the immobile partially consolidated bottom at z = 0 is referred to as a fluid mud layer which may exhibit a non-zero velocity when applied stresses exceed the cohesive yield stress. Thus the lutocline at z = m, between the fluid and the viscoplastic material, is not a no-slip boundary. For analytic purposes we shall assume that the lutocline at z = m is a stress free boundary much like a free surface, with the shear stresses resulting from fluid motion appearing in the stress field of the fluid mud layer itself. This assumption relieves the equations of motion for the velocity field of the jet on the fluid side of the interface from having to satisfy a no-slip condition at z = m. The no-slip boundary appears at the immobile partially consolidated bottom at z = 0. We shall assume there are minor

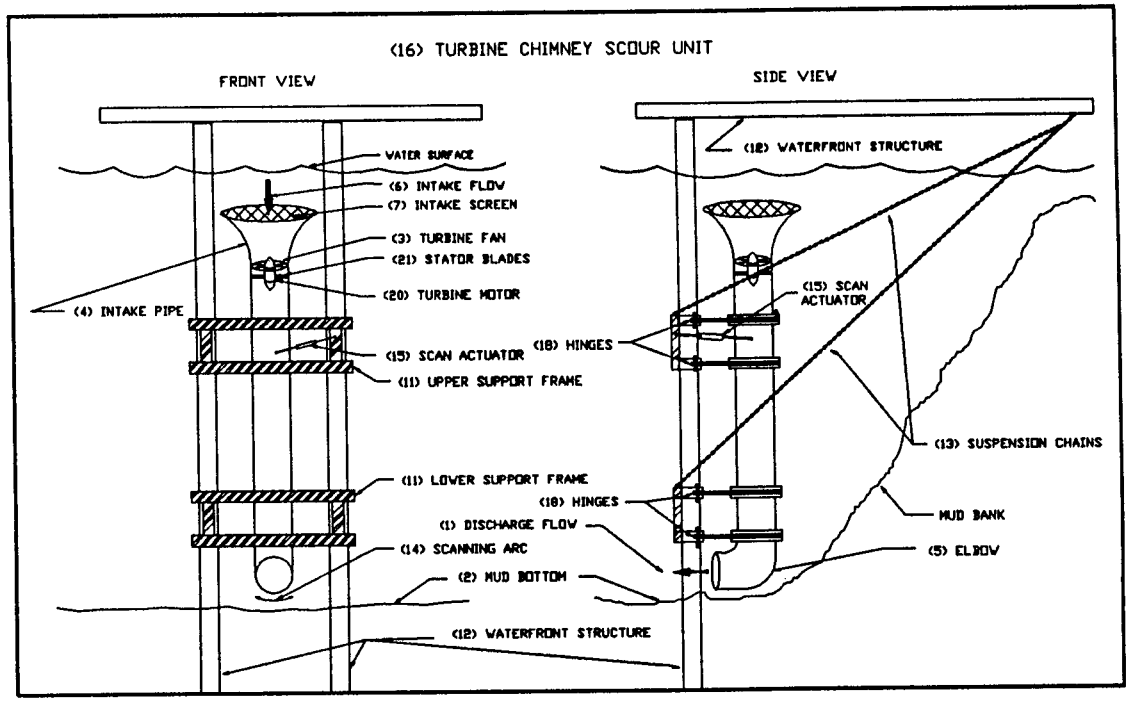

Figure 3. Conceptual diagram of the fluid bed interface as influenced by a generic hydrostatic jet.

irregularities along the surface $z = 0$ whose elevations are characteristically, z_0, where $z_0 << m$.

Below the fluid mud layer, $z < 0$, the sediment is at rest and there is a progressive buildup in sediment component density to some ultimate saturation value, $\rho = \rho_s$. This is due to consolidation and compaction under the weight of the overburden which proceeds at a rate characterized by $\rho_c K_s g$, where g is the acceleration of gravity and K_s is the sedimentation coefficient in seconds, Fugita (1962). The portion of the cohesive bottom below the fluid mud layer for which $\rho_c < \rho < \rho_s$ shall be referred to as the partially consolidated mud, which remains immobile.

Now superimpose a jet discharge across the lutocline surface at $z = m$. Assume this jet has operated a sufficient length of time for all transient pressure disturbances to propagate into the far field (the hydrostatic assumption). Therefore, along the axis of the jet we may assume a one-dimensional steady state in which upward diffusive mass fluxes due to the turbulent eddy transport of the jet are balanced by downward advective mass fluxes due to the settling of the suspended sediment under the influence of gravity, or:

$$\frac{\partial^2 \rho}{\partial z^2} = \frac{\omega_0}{\epsilon} \frac{\partial \rho}{\partial z} \tag{3}$$

Here ϵ is the eddy mass diffusivity which may approximated from mixing length theory as:

$$\epsilon = \frac{a k_0 \sqrt{\tau}}{\sqrt{\rho_m}} (z + z_0) \tag{4}$$

where k_0 is Von Karman's constant; τ is the jet induced shear stress; and a is the Peclet number, equal to a ratio of the mass diffusivity to the momentum diffusivity.

Equation (3) is solved by successive integrations subject to the following boundary conditions: (1) the jet will not entrain sediment from the fluid mud layer unless the applied jet stress, τ, exceeds the cohesive yield stress, τ_c, or $\rho = \rho_c$, at $z = m$ for $\tau < \tau_c$; and (2) $\rho = \rho_t$ at $z = h$ for $\tau \geq \tau_c$. A solution to Eq. (3) in the domain between the lutocline and the free surface subject to these boundary conditions is:

$$\rho = \frac{9 a^2 k_0^2 (\tau - \tau_c)}{\omega_0^2 \log^2[(z + z_0)/2z_0]} + \rho_c \exp\left[\frac{(z-m)}{(h-m)} \log \frac{\rho_t}{\rho_c}\right] \tag{5}$$

$$\text{for } \tau \geq \tau_c \text{ and } m \leq z \leq h$$

The first term on the right hand side of Eq. (5) is the disturbance to the sediment component density profile induced along the axis of the jet, while the second term represents the ambient density profile above the lutocline. The sediment component density above the lutocline is found to grow in direct proportion to the excess applied jet shear stress relative to the cohesive yield stress of the fluid mud layer, while decreasing with increasing particle size or increasing settling velocity.

Fine sediment deposition at the consolidated muddy bottom, z = 0 in Fig. 3, is directly proportional to the abundance of suspended sediment in the fluid mud layer, Ariathurai and Krone (1976) and Cole and Miles (1983). This abundance is determined by the net mass fluxes across the lutocline at z = m. The flux of suspended sediment entering the fluid mud layer due to settling under gravity is $-\rho\omega_0$. These downward directed settling fluxes are the predominant mass fluxes which occur across the lutocline in a dredged estuary. However in the presence of a turbulent jet, vertical transport due to eddy diffusion may become important, especially along strong density gradients in the neighborhood of the lutocline. The net of settling fluxes and diffusive fluxes across the lutocline determines the rate of change of suspended sediment in the fluid mud layer. However there is only a finite probability p(0,1), that this suspended sediment will actually stick to the bed at z = 0 and consolidate to some ultimate saturation density, ρ_s, see Krone (1962). Therefore the deposition flux, D, may be written:

$$D = \frac{-K_s\rho_c g + p(0,1)\left[\rho_c\omega_0 + \epsilon\frac{\partial\rho}{\partial z}\Big|_{z=m}\right]}{(1 - \rho_c/\rho_s)} \tag{6}$$

In Eq. (6) positive values of D correspond to deposition while negative values indicate entrainment of suspended sediment from the fluid mud layer into the floc layer and fluid above. In the absence of jet induced shear stresses, ($\tau < \tau_c$ as in control areas) the diffusive flux term in Eq. (6) is negligable and the deposition flux becomes a positive value controlled by local settling fluxes, $\rho_c\omega_0$. If, however, jet induced shear stresses become large, $\tau \geq \tau_c$, then a large negative diffusive flux term arises in Eq. (6) which we refer to as the jet entrainment flux, E_j, or:

$$E_j = \frac{-K_s\rho_c g + p(0,1)\left\{ - \mathrm{Re}\left[\frac{9a^3k_0^3(\tau-\tau_c)^{3/2}(m+z_0)}{\omega_0^2 z_0\sqrt{\rho_m}}\log\left[\frac{m+z_0}{2z_0}\right]\right]\right\}}{(1 - \rho_c/\rho_s)} \tag{7}$$

where Re is the real part operator. Hence there is no jet entrainment flux when $\tau < \tau_c$. From Eq. (7) it is clear that the variation of the jet entrainment flux

along the jet axis depends decisively on the decay rate of the applied jet shear stress with distance from the jet discharge, and upon the cohesive yield stress of the fluid mud layer.

Applied Jet Shear Stress

A laboratory experiment was conducted in which a turbulent jet was discharged across a plain immobile bottom imbedded with a flush mounted shear stress probe. The position of the flush mounted shear stress probe was varied along the axis of the jet. The initial discharge velocity of the jet, U_0 was varied for several different jet diameters, d. The results were found through regression analysis to produce a systematic power law relation between the applied jet shear stress τ, and the distance, x, along the jet axis from the jet discharge. These results are plotted in Fig. 4. The regression line for the data was found to obey the following:

$$\tau = 120\rho_m U_0^2 \left(\frac{U_0 d}{\nu}\right)^{-0.4} \left(\frac{d}{x}\right)^{2.4} \tag{8}$$

We find that the applied jet shear strength decays as the -2.4 power of the distance, x, from the jet discharge point. The flush mounted shear stress probe indicated that lines of constant stress resemble teardrops as diagrammed in

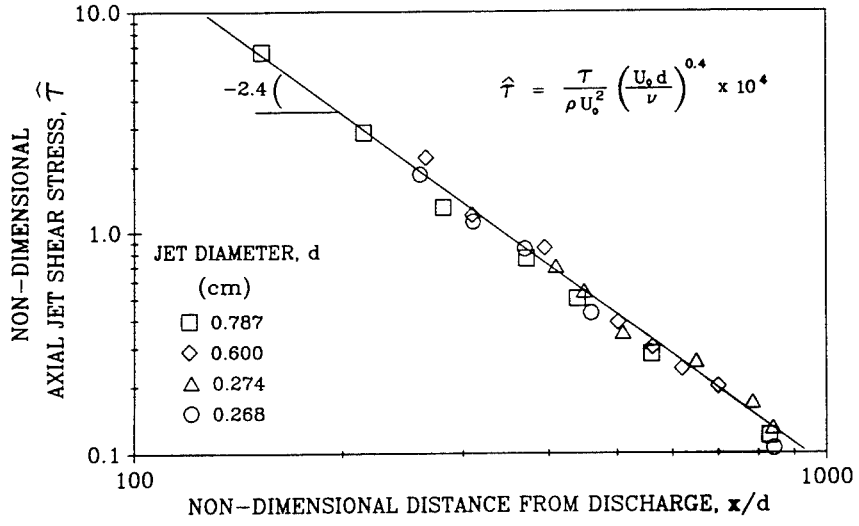

Figure 4. Extinction rate of applied jet shear stress measured on laboratory scales.

Fig. 3. The maximum width of each teardrop occurred at roughly 2/3 the maximum range from the jet for any given contour of constant stress. The width of the teardrop was found to be approximately 1/3 the maximum range of the shear stress contour. Our focus herein is along the jet axis for which the maximum range, X_m, for any given contour of constant applied jet shear stress, τ, is given by:

$$X_m = d\left[\frac{\tau R_j^{0.4}}{120\rho_m U_0^2}\right]^{-0.417} \tag{9}$$

where R_j is the jet Reynolds number = $U_o d/\nu$.

In Fig. 5, plots of Eq. (9) show that the maximum axial range of any given stress contour increases either with increasing axial jet discharge velocity or increasing jet diameter. In otherwords, X_m grows with increasing jet flow rate, $U_0\pi d^2/4$. Equation (7) indicates that the particular value of applied stress, τ, must exceed the cohesive yield stress , τ_c, in order to effect deposition out to X_m. Consequently we find in Fig. 5 that X_m decreases for any given selection of U and d with increasing strength of the fluid mud.

Cohesive Yield Stress of the Fluid Mud Layer

Because the steady state jet plume must induce motion of the fluid mud layer to effect entrainment, the decisive question is whether the applied jet shear stress exceeds the cohesive yield stress in the fluid mud layer. To assess the strength of the fluid mud, grab samples were gathered by diver in the neighborhood of the consolidated bottom. Hydrometer analysis determined that the sediments in the fluid mud layer were 25% clay, 55% silt and 20% fine sand with an organic content of 4%. X-ray diffraction revealed that the predominant minerals present in the fluid mud layer were montmorillonite, illite, and kaolinite. The cohesive yield stress was determined with a Brookfield synchro-electric viscometer equipped with a special UL adapter, (Brookfield Engineering Laboratories Inc, Stoughton, MA). The usefulness of the instrument in predicting this behavior of cohesive sediments both in the field and in the laboratory has been described in detail by Faas (1990). The coaxial cylinder geometry of the UL adapter provides greater sensitivity for low viscosity suspensions and the instrument is accurate to within 1% of the full scale reading.

The grab samples from the fluid mud layer were washed with deionized water to remove sea salts, followed by screening to remove pieces of debris, shells, etc. The samples were than sieved through a 62 micron sieve to separate the fine fraction from the coarse fraction. Subsequently the suspension was agitated thoroughly to break up any large clumps or flocs. The suspension was then

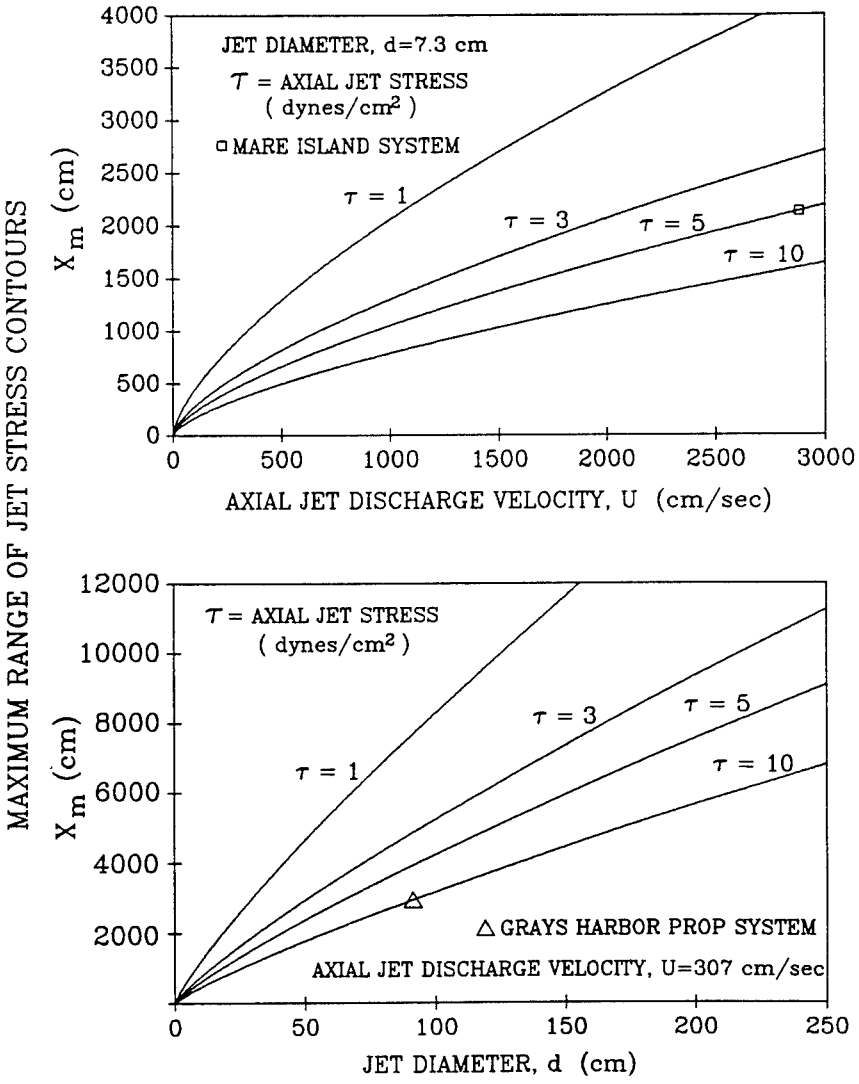

Figure 5. Dependence of the maximum range of applied jet shear stress upon: a) axial discharge velocity (jet diameter/ the Mare Island pump based system); and b) jet diameter (axial jet discharge velocity/ the propeller based Grays Harbor jet system). Symbols indicate design points for prototype tests shown in Fig. 8.

sheared in the Brookfield viscometer. The initial reading was taken at zero salinity. Subsequent readings were taken at increasing salinities of up to 30 o/oo. Three separate runs were made on the same sediment suspension and 3 or 4 viscometer readings were taken for each increment of salinity. There were no variations in the measured values for all three runs thereby assuring the accuracy of the viscometer to produce data of good quality.

Two sets of experiments were conducted. One consisted of analyzing the yield stress behavior of the natural sediment sample and the other measured the yield stress after removing the organic matter. The organic matter was removed by treating the sediment sample with 30% hydrogen peroxide solution. The sediment component density was then calculated from the ratio of the oven-dried weight of the sample to the total volume of the sediment suspension.

The yield stress was measured at a fixed sediment concentration while the salinity was varied in increments of 5 o/oo. The experiments were then repeated for varying sediment concentrations. The results show that as the salinity is increased from 0 to 5 o/oo, there is a sharp increase in cohesive yield stress followed by a gradual increase beyond 5 o/oo, see Fig. 6. This result is in agreement with the results of previous investigators in the lower salinity range, see Edzwald et al. (1974), Gibbs (1983). However, even after 5 o/oo, the yield stress does not level off but continues to increase at higher salinities. This result implies that the pump intakes should be placed as close to the surface as possible, to draw off the lens of low salinity surface water. The resulting reduction in yield stress within the low salinity jet plume would then, by Eq. (9), maximize the range of deposition reduction.

Several runs of experiments were conducted in the sediment concentration range of 10 grams/liter to 75 grams/liter. This range is representative of the seasonal variations in fluid mud layers at the prototype test sites at Mare Island, CA and Grays Harbor, WA, see Jenkins et al. (1980). The values of yield stress obtained were 0.85 dynes/cm^2 at 10 grams/liter and zero salinity up to 5 dynes/cm^2 at 75 grams/liter and 30 o/oo. The yield stress in Fig. 6 for the sediment concentration of 75 grams/liter rises from 1.5 dynes/cm^2 at zero salinity to 4.26 dynes/cm^2 at 3 o/oo and finally to 5.06 dynes /cm^2 at 30 o/oo. There is a 19% increase in yield stress from 3 o/oo to 30 o/oo. Similarly, other runs show a percentage increase of 15 to 20 % as the salinity increases from 3 to 30 o/oo. The sediment without the organic matter (Fig. 6) shows the same trend as the natural sediments, indicating that the organic matter is not playing a significant role in affecting the yield stress increase due to the effects of salinity.

Jet Experiments in the Field

Jet experiments were conducted at three west coast sites: (1) Mare Island, California; (2) Terminal 4, Grays Harbor, Washington; (3) Terminal 2, Grays Harbor Washington. The Mare Island jet system was a pump based system

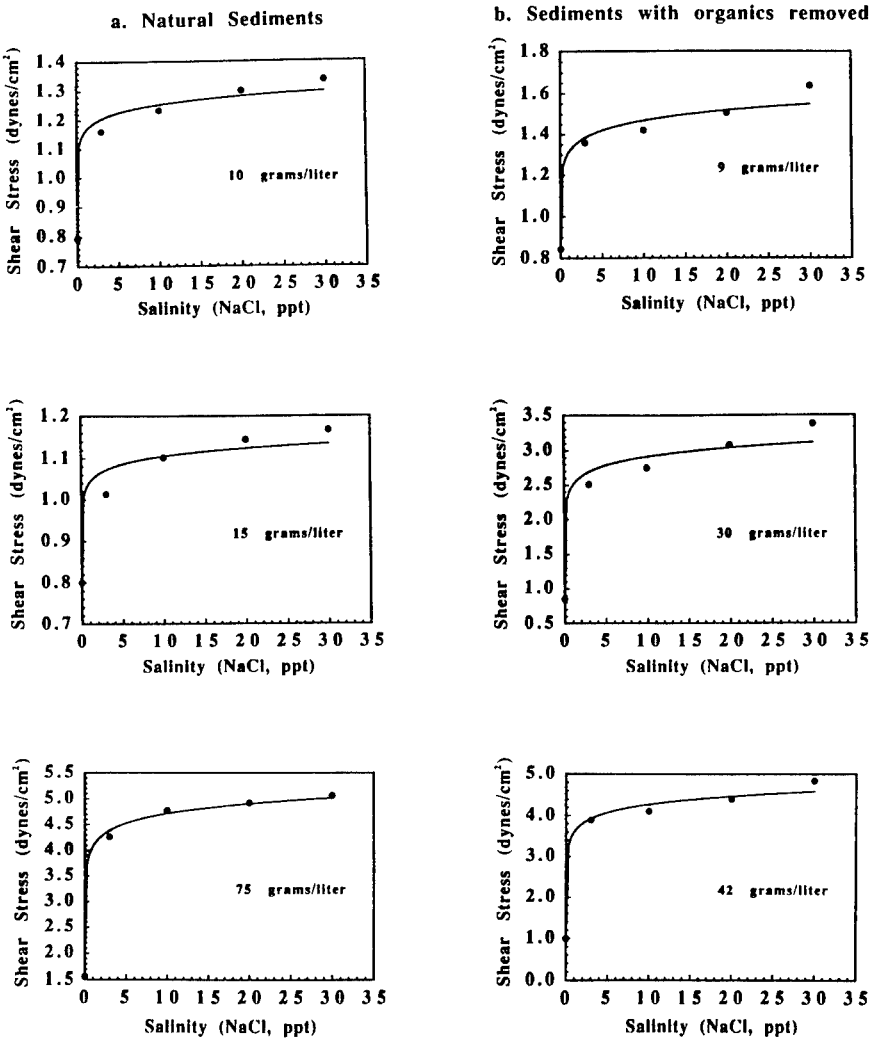

Figure 6. Cohesive yield stress dependence upon salinity and concentration. Right hand column figures are based upon sediment samples with the organics removed. Left hand column figures are based upon natural sediments with the organic content intact.

comprised of ten jets at 914 cm spacings, each with a diameter of 7.3 cm and a discharge velocity of 2,879 cm/sec. Two distinctly different jetting systems were tested at Grays Harbor, Washington. The Terminal 4 system was pump based, as shown in Fig. 1, comprised of 24 jets at 914 cm spacings, each with a diameter of 22.2 cm and a discharge velocity of 2,207 cm/sec. The Terminal

2 system was a propeller based system as diagrammed in Fig. 2 comprised of a single discharge with a 91.4 cm diameter and a 307 cm/sec discharge velocity.

Based upon cohesive yield stress results like those in Fig. 6, the Mare Island system was designed to produce an applied shear stress of 5 dynes/cm^2 out to a maximum range of 2,000 cm, to allow for seasonal maximums in suspended sediment. The settling velocity of the flocs in the fluid mud layer was determined to be 0.035 cm/sec with typical excess densities in the fluid mud layer of 0.075 g/cm^3. The saturation density of the consolidated muds at Mare Island was determined to be 1.1 g/cm^3. Dynamic shear stress analyses at Grays Harbor revealed significantly stronger fluid mud layers as thick as 150 cm with cohesive yield stresses as high as 10 dynes/cm^2. The flocs of these fluid mud layers were larger with median settling velocities of 0.05 cm/sec. Typical excess densities in the fluid mud layer at Grays Harbor were found to be 0.1 g/cm^3 with saturated densities for the consolidated material on the order of 1.1 g/cm^3. Accordingly, the design applied shear stress for both the Grays Harbor jetting systems was increased to 10 dynes/cm^2 out to a maximum range of 3,000 cm. The design point for the Mare Island system is indicated in Fig. 5a while the design point for the propeller based Grays Harbor system is shown in Fig. 5b.

Fathometer surveys were conducted over a 2 month period at Mare Island and over 2 separate 3 month periods at Grays Harbor. Comparisons between the local depths in the jetting areas to those in control areas were used to calculate the jet entrainment flux by the following:

$$E_j = \rho_s \frac{\eta_{jet} - \eta_{control}}{\Delta t} \simeq D_{jet} - D_{control} \qquad (10)$$

where η was the vertical position of the immobile bed as determined from 40 kHz fathometer soundings in the test areas and control areas, respectively. The jet entrainment flux is a measure of the deposition flux which did not occur due to the action of the jet stress over a period of time, Δt. Figure 7 shows a bathymetry contour plot from the survey of the Terminal 4 pump based Grays Harbor system conducted between March 1987 and June 1987. These soundings were conducted along 2,000 feet of waterfront, one half of which (along the upstream portion) served as a control area. Seven hundred feet of the downstream portion was influenced by a 700 ft long reach of 24 jets. It is clear from these bathymetry surveys that the jets had a pronounced effect on preventing deposition. The entire 610 meters of waterfront was dredged to -11.6 meters MLLW just before the activation of the jetting systems in March 1987. By June 1987 the control area had shoaled to between -7 and -8 MLLW while major portions of the jet test area inside 30 meters were maintained at the original dredged depths. Surprisingly, deposition was retarded as far out as 42 meters from the jet discharge nozzles.

Measured jet entrainment fluxes from the average depths over control areas and jet test areas according to Eq. (10) are plotted in Fig. 8 and compared against entrainment flux calculations based on Eq. (7) for the respective jet and

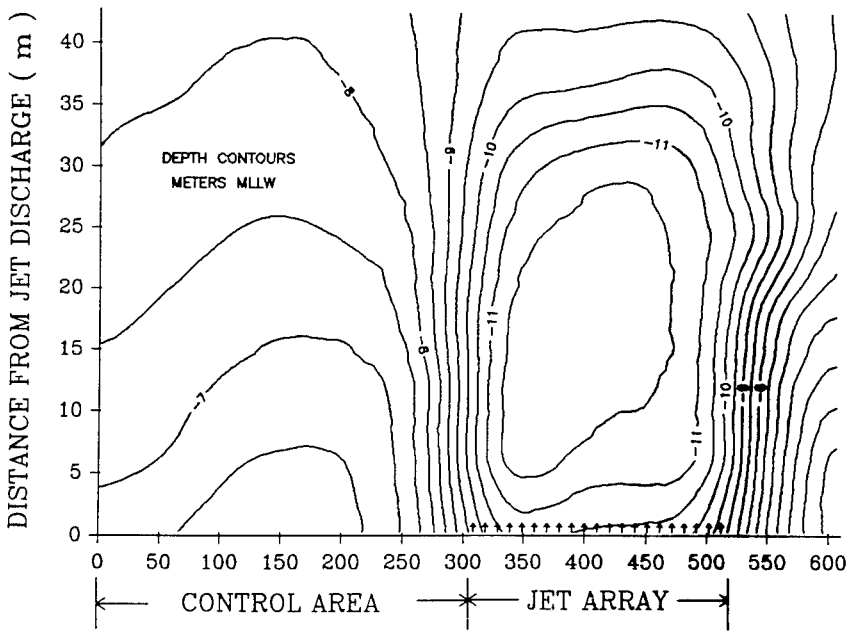

Figure 7. Bathymetry survey at the end of the test period of the pump based Grays Harbor jet system conducted between March 1987 and June 1987. Bathymetry contours are based upon echo soundings of a 40 kHz fathometer. Ebb flow proceeds from left to right with the control area situated on the upstream side during jet operations in ebbing flow arrows indicate the position of individual jets.

sediment properties listed. The value for the probability factor, p(0,1), was adjusted to achieve best fit between the calculations and the data. Even then, it was necessary to base the calculations on cohesive yield stress values less then the design values in order to account for the non zero entrainment fluxes measured at great distances from the discharge points. The entrainment flux data suggests that the cohesive yield stress values during the tests were effectively only about 1 and 4 dynes/ cm^2 at MINSY and Grays Harbor respectively. However, these values are consistent with the results of Fig. 6, for artificially depressed salinities which would arise in the field from the jet discharges which derive their drive water from intakes near the surface.

Conclusion

The results indicate that deposition of fine grain sediments may be controlled through the semi-diurnal application of hydrostatic jets producing applied shear

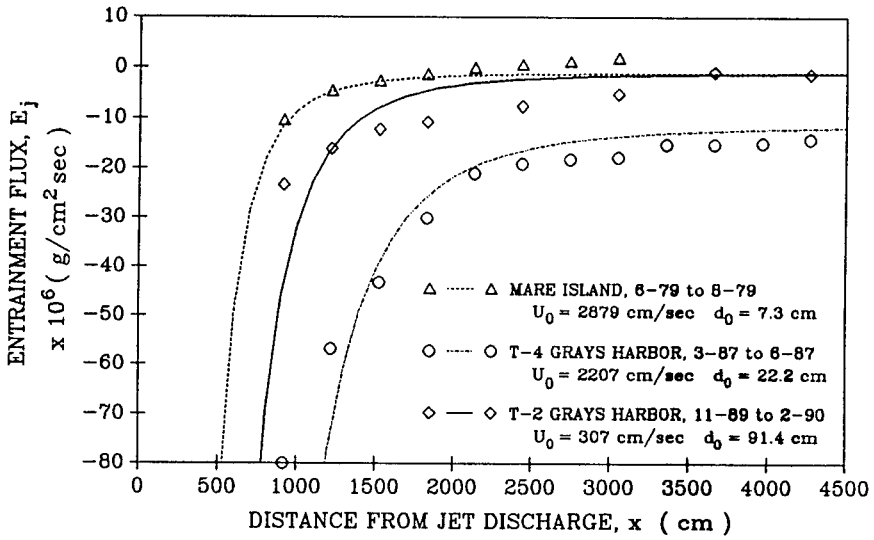

Figure 8. Measured deposition fluxes derived from spatial averages of fathometer surveys as compared with calculated deposition fluxes based on Eq. (7). The dotted curve represents the theoretical entrainment expected from the pump based jet array system at Mare Island Naval Shipyard using the following parameterization: p = 0.001, z_0 = 1 cm, m = 10 cm, and a = 0.002. The solid curve is the theoretical entrainment expected from the turbine chimney unit at Terminal 2, of the Port of Grays Harbor, WA, using the following values: p = 0.0000005, z_0 = 10 cm, m = 150 cm, and a = 0.02. The dashed-dotted curve corresponds to the theoretical predictions of the performance of the pump based jet array system at Terminal 4, the Port of Grays Harbor, WA, with parameterization as follows: p = 0.0002, z_0 = 10 cm, m = 150 cm, and a = 0.0036.

stresses in excess of the cohesive yield stress of the fluid mud layer. This may be accomplished by either of two means: (1) application of high velocity jets or (2) application of large diameter jets. By either approach the effect of controlling deposition thru jet entrainment in the far field is maximized by maximizing the total jet flow rate. This suggests that the total eddy momentum content of the jet discharge is the limiting factor in facilitating entrainment and hence controlling deposition. In other words the turbulent momentum of the jet discharge is progressively diluted with increasing distance from the jet discharge point. At some maximum range, the eddy momentum of the jet discharge is diluted to such an extent that it is incapable of entraining sediment from the fluid mud layer across the lutocline interface. The unexpected persistence of this entrainment in the far field of low salinity jets also suggests that the jet salinity

may exert a modifying effect on the cohesive yield stress of the fluid mud, rendering it more susceptible to eddy transport across the lutocline.

Acknowledgements

The authors wish to thank Dr. James A. Bailard for his many contributions to this work throughout its duration. We further wish to thank Mr. Joseph Sparks of the Mare Island divers for numerous contributions of effort and mechanical innovation in the Mare Island jet array design and maintenance. This work was supported in part by the Office of Naval Research Ocean Engineering Division, Code 1121.

References

Ariathurai, R., and R.B. Krone, Finite element model of cohesive sediment transport, *J. Hydraul. Div.* ASCE, 102(HY3), 323-338, 1976.

Bailard, J.A., and S.A. Jenkins, Method and apparatus for the active prevention of sedimentation in harbors and waterways, U.S. Patent #4,957,392, 1990.

Cole, P., and G.V. Miles, Two-dimensional model of mud transport. *J. Hydraul. Eng.* ASCE, 109(1), 1-12, 1983.

Dyer, K.R., *Coastal and Estuarine Sediment Dynamics*, 342 pp, Wiley, New York, 1985.

Edzwald, J.K., J.B. Church, and C.R. O'Melia, Coagulation in estuaries, *Envir. Sci. and Tech.* 8, 58-63, 1974.

Faas, R.W., A portable rotational viscometer for field and laboratory analysis, *J. Coast. Res.* 735-738, 1990.

Fugita, H., *Mathematical Theory of Sedimentation Analysis*, 315 pp, Academic, York, 1962.

Gibbs, R.J., Coagulation rates of clay minerals and natural sediments, *J. Sedimentary Petrology*, 53, 1193-1203, 1983.

Heinz, R.A., J.A. Bailard, and S.A. Jenkins, Water jets fight silt, *Civil Engineering*, 59(1), 54-58, 1989.

Jenkins, S.A., D.L. Inman and J.A. Bailard, Opening and maintaining tidal lagoons and estuaries, *Proc. 7th Int Coastal Eng Conf*, Amer. Soc. Civil Eng, 2, 1528-1547, 1980.

Jenkins, S.A. and J.A. Bailard, Anti-sedimentation system for harbors, *World Wide Shipping*, 52(1), 70-75, 1989.

Krone, R.B., *Flume Studies of the Transport of Sediment in Estuarial Shoaling Processes*, Final report, Hydraulics Engineering Laboratory and Sanitary Engineering Research Laboratory, University of California, Berkeley, 1962.

Krone, R.B., Aggregation of suspended particles in estuaries. *In: Estuarine Transport, Process*, B. Kjerfve, (ed.). University of South Carolina Press, Columbia, SC, 177-190, 1978.

Mehta, A.J., On estuarine cohesive sediment suspension behavior, *J. Geophys. Res.*, 94, (C10), 14,303-14,314, 1989.

Mehta, A.J., and E. Partheniades, An investigation of the depositional properties of flocculated fine sediments. *J. Hydraul. Res.* 13(4), 361-381, 1975.